
The Representation Jensen-Shannon Divergence

Jhoan K. Hoyos-Osorio, Santiago Posso-Murillo & Luis G. Sanchez-Giraldo
Department of Electrical and Computer Engineering
University of Kentucky
Lexington, USA
{keider.hoyos, spo, luis.sanchez}@uky.edu

Abstract

Statistical divergences quantify the difference between probability distributions, thereby allowing for multiple uses in machine-learning. However, a fundamental challenge of these quantities is their estimation from empirical samples since the underlying distributions of the data are usually unknown. In this work, we propose a divergence inspired by the Jensen-Shannon divergence which avoids the estimation of the probability density functions. Our approach embeds the data in an reproducing kernel Hilbert space (RKHS) where we associate data distributions with uncentered covariance operators in this representation space. Therefore, we name this measure the representation Jensen-Shannon divergence (RJSD). We provide an estimator from empirical covariance matrices by explicitly mapping the data to an RKHS using Fourier features. This estimator is flexible, scalable, differentiable, and suitable for minibatch-based optimization problems. Additionally, we provide an estimator based on kernel matrices without an explicit mapping to the RKHS. We provide consistency convergence results for the proposed estimator. Moreover, we demonstrate that this quantity is a lower bound on the Jensen-Shannon divergence, leading to a variational approach to estimate it with theoretical guarantees. We leverage the proposed divergence to train generative networks, where our method mitigates mode collapse and encourages samples diversity. Additionally, RJSD surpasses other state-of-the-art techniques in multiple two-sample testing problems, demonstrating superior performance and reliability in discriminating between distributions.

1 Introduction

Divergences quantify the difference between probability distributions. In machine-learning, divergences can be applied to a wide range of tasks, including generative modeling (generative adversarial networks, variational auto-encoders), two-sample testing, anomaly detection, and distribution shift detection. The family of f -divergences is among the most popular statistical divergences, including the well-known Kullback-Leibler and Jensen-Shannon divergences. A fundamental challenge to using divergences in practice is that the underlying distribution of data is unknown, and thus divergences must be estimated from observations. Several divergence estimators have been proposed (Yang & Barron, 1999; Sriperumbudur et al., 2012; Krishnamurthy et al., 2014; Moon & Hero, 2014; Singh & Póczos, 2014; Li & Turner, 2016; Noshad et al., 2017; Moon et al., 2018; Bu et al., 2018; Berrett & Samworth, 2019; Liang, 2019; Han et al., 2020; Sreekumar & Goldfeld, 2022), most of which fall into four categories: plug-in, kernel density estimation, k -nearest neighbors, and neural estimators.

Kernel methods are another approach for measuring the interaction between probability distributions. For example, the maximum mean discrepancy (MMD) (Gretton et al., 2012) is a divergence computed as the distance between the mean embeddings (first-order moments) of the two probability

distributions in a reproducing kernel Hilbert space (RKHS). However, due to the underlying geometry, MMD lacks a straightforward connection with classical information theory tools (Bach, 2022). On the other hand, covariance operators (second-order moments) in RKHS have been used to propose multiple information theoretic quantities, such as marginal, joint, and conditional entropy (Sanchez Giraldo et al., 2014), as well as mutual information (Yu et al., 2019), and total correlation (Yu et al., 2021). However, strategies for estimating divergences within this framework have been less explored.

To fill this void, we propose a kernel-based information theoretic learning framework for divergence estimation. We make the following contributions:

- A novel divergence, the representation Jensen-Shannon divergence (RJSD), that avoids the estimation of the underlying density functions by mapping the data to an RKHS where distributions can be embedded using uncentered covariance operators acting in this representation space.
- An estimator from empirical covariance matrices that explicitly map data samples to an RKHS using Fourier features. This estimator is flexible, scalable, differentiable, and suitable for minibatch-based optimization problems. Additionally, an estimator based on kernel matrices without an explicit mapping to the RKHS is provided. Consistency results and sample complexity bounds for the proposed estimator are derived.
- A connection between the kernel-based entropy and Shannon’s entropy, as well as the relationship between RJSD with the classical Jensen-Shannon divergence. Namely, RJSD emerges as a lower bound on the classical Jensen-Shannon divergence enabling the construction of a variational estimator for the classical Jensen-Shannon divergence with statistical guarantees.

We use RJSD for training generative adversarial networks and show that it prevents mode collapse and encourages diversity, leading to more accurate and heterogeneous results. We also apply RJSD for two-sample testing problems and show that it accurately detects differences between probability distribution functions even for cases where other state-of-the-art measures fall short.

2 Background

2.1 Mean embeddings and Covariance operators

Let $\{\mathcal{X}, \mathbf{B}_{\mathcal{X}}\}$ be a measurable space and $\kappa : \mathcal{X} \times \mathcal{X} \rightarrow \mathbb{R}_{\geq 0}$ be a positive definite kernel. There exists a mapping $\phi : \mathcal{X} \rightarrow \mathcal{H}$, where \mathcal{H} is a reproducing kernel Hilbert space (RKHS), such that $\kappa(x, x') = \langle \phi(x), \phi(x') \rangle_{\mathcal{H}}$. The kernel mean embedding (Muandet et al., 2017) is a mapping μ from $\mathcal{M}_+^1(\mathcal{X})$ to \mathcal{H} , where $\mathcal{M}_+^1(\mathcal{X})$ is the space of probability measures on \mathcal{X} . The kernel mean embedding is defined as follows:

$$\mu_{\mathbb{P}} = \mathbb{E}_{X \sim \mathbb{P}}[\phi(X)] = \int_{\mathcal{X}} \phi(x) d\mathbb{P}(x), \text{ for } \mathbb{P} \in \mathcal{M}_+^1. \quad (1)$$

An important property of the mean embedding is that if $\mathbb{E}_{X \sim \mathbb{P}}[\kappa(X, X)] < \infty$, for any $f \in \mathcal{H}$, then $\mathbb{E}_{X \sim \mathbb{P}}[f(X)] = \langle f, \mu_{\mathbb{P}} \rangle_{\mathcal{H}}$.

Another related mapping is the uncentered covariance operator. In this case, $\mathbb{P} \in \mathcal{M}_+^1$ is mapped to an operator $C_{\mathbb{P}} : \mathcal{H} \rightarrow \mathcal{H}$ given by:

$$C_{\mathbb{P}} = \mathbb{E}_{X \sim \mathbb{P}}[\phi(X) \otimes \phi(X)] = \int_{\mathcal{X}} \phi(x) \otimes \phi(x) d\mathbb{P}(x). \quad (2)$$

Similarly, for any $f, g \in \mathcal{H}$, $\mathbb{E}_{X \sim \mathbb{P}}[f(X)g(X)] = \langle g, C_{\mathbb{P}}f \rangle_{\mathcal{H}}$. For a bounded kernel, the covariance operator is positive semi-definite, Hermitian (self-adjoint), and trace class (Sanchez Giraldo et al., 2014; Bach, 2022). The spectrum of the covariance is discrete and consists of non-negative eigenvalues λ_i with $\sum \lambda_i < \infty$.

2.2 Kernel-based information theory

We can define information theoretic quantities on the spectrum of normalized covariance operators with unit trace. This observation was made by Sanchez Giraldo et al. (2014) who proposed the kernel-based entropy functional: $S_{\alpha}(C_{\mathbb{P}}) = \frac{1}{1-\alpha} \log [\text{Tr}(C_{\mathbb{P}}^{\alpha})]$. $\text{Tr}(\cdot)$ denotes the trace operator, and $\alpha > 0$ is the entropy order. This quantity resembles quantum Rényi entropy (Müller-Lennert et al., 2013) where the covariance operator play the role of a density matrix. In the limit when $\alpha \rightarrow 1$, $S_{\alpha \rightarrow 1}(C_{\mathbb{P}}) = -\text{Tr}(C_{\mathbb{P}} \log C_{\mathbb{P}})$ becomes von Neumann entropy. This connection between covariance operators in RKHS and information theory has been also discussed by Bach (2022).

Kernel-based entropy estimator: The kernel-based entropy estimator relies on the spectrum of the empirical uncentered covariance operator, which is defined as $\mathbf{C}_X = \frac{1}{N} \sum_{i=1}^N \phi(x_i) \otimes \phi(x_i)$. Let $\mathbf{X} = \{x_i\}_{i=1}^N$ be a set of samples $x \in \mathcal{X}^d$ following an unknown distribution \mathbb{P} defined on \mathcal{X}^d . Then, we can construct the Gram matrix \mathbf{K}_X , consisting of all normalized pairwise kernel evaluations of the samples in \mathbf{X} , that is $(\mathbf{K})_{ij} = \kappa(x_i, x_j)$. If we normalize the matrix \mathbf{K}_X such that, $\text{Tr}(\mathbf{K}_X) = 1$, \mathbf{C}_X and \mathbf{K}_X have the same non-zero eigenvalues (Sanchez Giraldo et al., 2014). This construction yields the kernel-based entropy estimator:

$$S(\mathbf{K}_X) = -\text{Tr}(\mathbf{K}_X \log \mathbf{K}_X) = -\sum_{i=1}^N \lambda_i \log \lambda_i, \quad (3)$$

where λ_i represents the i th eigenvalue of \mathbf{K}_X . However, this eigen-decomposition has $\mathcal{O}(N^3)$ time complexity, restricting the use of the kernel-based estimator in applications involving large number of samples.

Covariance-based estimator: Alternatively, we can use an explicit mapping $\phi : \mathcal{X}^d \rightarrow \mathcal{H}^D$ to a finite dimensional RKHS. We propose to use Fourier features to construct a mapping function to \mathcal{H}^D . Given a shift-invariant kernel $\kappa : \mathcal{X} \times \mathcal{X} \rightarrow \mathbb{R}_{\geq 0}$, the random Fourier features (RFF) (Rahimi & Recht, 2007) is a method to create a smooth feature mapping $\phi_\omega(x) : \mathcal{X}^d \rightarrow \mathbb{R}^D$ so that $\kappa(x, x') \approx \langle \phi_\omega(x), \phi_\omega(x') \rangle$. To generate an RFF mapping, we compute the Fourier transform of the kernel, $p(\omega) = \frac{1}{2\pi} \int e^{-j\omega^\top \delta} \kappa(\delta) d\delta$, which yields a probability distribution function. From this distribution, we draw $\frac{D}{2}$ i.i.d samples $\omega_1, \dots, \omega_{D/2} \in \mathbb{R}^d$. Finally, the mapping is given by $\phi_\omega(x) = \sqrt{\frac{2}{D}} \left[\cos(\omega_1^\top x), \sin(\omega_1^\top x), \dots, \cos(\omega_{D/2}^\top x), \sin(\omega_{D/2}^\top x) \right]$.

Letting $\Phi_X \in \mathbb{R}^{N \times D}$ be the matrix containing the mapped samples, we can compute the empirical uncentered covariance matrix as $\mathbf{C}_X = \frac{1}{N} \Phi_X^\top \Phi_X$. Finally, we exploit the spectrum of the uncentered covariance matrix to compute the von Neumann entropy of \mathbf{C}_X as:

$$S(\mathbf{C}_X) = -\text{Tr}(\mathbf{C}_X \log \mathbf{C}_X) = -\sum_{i=1}^D \lambda_i \log \lambda_i, \quad (4)$$

where λ_i represents the i th eigenvalue of \mathbf{C}_X . This eigendecomposition has $\mathcal{O}(D^3)$ time complexity, where D is independent of the sample size and thus scalable.

The kernel-based entropy has been used as a building block for other matrix-based measures, such as joint and conditional entropy, mutual information (Yu et al., 2019), total correlation (Yu et al., 2021), and divergence (Hoyos Osorio et al., 2022). Despite the success of the aforementioned measures, their connection with the classical information theory counterparts remains unclear.

Next, we investigate the relationship between the kernel-based entropy estimator and Shannon's entropy.

Definition 1. Let $\phi : \mathcal{X} \rightarrow \mathcal{H}$ be a mapping to a reproducing kernel Hilbert space (RKHS), and $\kappa : \mathcal{X} \times \mathcal{X} \rightarrow \mathbb{R}_{\geq 0}$ be a positive definite kernel, such that $\kappa(x, x') = \langle \phi(x), \phi(x') \rangle_{\mathcal{H}}$, and $\kappa(x, x) = 1$ for all $x \in \mathcal{X}$. Then, the **kernel density function** induced by the mapping ϕ is defined as follows:

$$\mathbb{P}_\phi(x) = \frac{1}{h} \langle \phi(x) | C_{\mathbb{P}} | \phi(x) \rangle = \frac{1}{h} \int_{\mathcal{X}} \kappa^2(x, x') d\mathbb{P}(x'), \quad (5)$$

where $h = \int_{\mathcal{X}} \langle \phi(x) | C_{\mathbb{P}} | \phi(x) \rangle dx$ is the normalizing constant.

Eqn. 5 can be interpreted as an instance of the Born rule which calculates the probability of finding a state $\phi(x)$ in a system described by the covariance operator $C_{\mathbb{P}}$ (González et al., 2022). Equivalently, the right hand side corresponds to a Parzen density estimator with kernel $\kappa^2(\cdot, \cdot)$.

Theorem 1. Let $\mathbb{P}_\phi(x)$ be the kernel density function induced by a mapping $\phi : \mathcal{X} \rightarrow \mathcal{H}$, then, the cross entropy between \mathbb{P} and \mathbb{P}_ϕ is:

$$H(\mathbb{P}, \mathbb{P}_\phi) = S(C_{\mathbb{P}}) + \log(h). \quad (6)$$

Proof: See Appendix A.1.

This result relates to kernel-density estimation for entropy calculation; however, the covariance operator bypasses the estimation of the underlying distribution. Consequently, we can use well-known results about the convergence of the kernel-density estimator. Let $\hat{\mathbb{P}}_\gamma(x)$ be the empirical kernel density function by a Gaussian kernel with scale parameter γ . Dmitriev & Tarasenko (1974) demonstrate that $H(\hat{\mathbb{P}}_\gamma)$ converges to $H(\mathbb{P})$ as both, N and $\gamma \rightarrow \infty$, with probability one. Notice, that in the limit when $\gamma \rightarrow \infty$, $\kappa(x, x') = 0$ for all $x \neq x'$, and therefore, $h \rightarrow 1$, leading to $H(\mathbb{P}) = S(C_{\mathbb{P}})$ which proves the convergence of the kernel-based entropy. A similar result can be proved for empirical covariance operators generated through RFFs.

Theorem 2. *Let $\phi_\omega : \mathcal{X}^d \rightarrow \mathbb{R}^D$ be a Fourier feature mapping approximating the Gaussian kernel with scale parameter $\frac{\gamma}{2} \rightarrow \infty$ as $N \rightarrow \infty$, and let C_X be the empirical covariance matrix for N samples. Then, there exists constants C_1 and C_2 such that:*

$$\Pr \{ |H(\mathbb{P}) - (S(C_X) + \log(h_\gamma))| < \epsilon \} > 1 - \max \{ P_1(N; \epsilon), P_2(D; \epsilon) \}, \quad (7)$$

where $P_1(N; \epsilon) = C_1 \exp\left(-\frac{C_2 \epsilon^2 N^{\frac{1}{10}}}{16}\right)$, and $P_2(D; \epsilon) = 2^8 \left(\frac{\sqrt{d\gamma} h_\gamma \text{diam}(\mathcal{X})}{\epsilon}\right)^2 \exp\left(\frac{-D\epsilon^2}{h_\gamma^2(d+2)}\right)$.

Proof: See Appendix A.2.

Similar to the Gaussian kernel, in the limit when N, D and $\gamma \rightarrow \infty$, $\langle \phi_\omega(x), \phi_\omega(x') \rangle = 0$ for all $x \neq x'$, and therefore, $h_\gamma \rightarrow 1$, leading to $H(\mathbb{P}) = S(C_X)$ which demonstrates the convergence of the covariance-based entropy.

3 Representation Jensen-Shannon Divergence

For two probability measures \mathbb{P} and \mathbb{Q} on a measurable space $\{\mathcal{X}, \mathbf{B}_{\mathcal{X}}\}$, the Jensen-Shannon divergence (JSD) is defined as follows:

$$D_{JS}(\mathbb{P}, \mathbb{Q}) = H\left(\frac{\mathbb{P} + \mathbb{Q}}{2}\right) - \frac{1}{2}(H(\mathbb{P}) + H(\mathbb{Q})), \quad (8)$$

where $\frac{\mathbb{P} + \mathbb{Q}}{2}$ is the mixture of both distributions and $H(\cdot)$ is Shannon's entropy. Properties of JSD, such as boundedness, convexity, and symmetry have been extensively studied (Briët & Harremoës, 2009; Sra, 2021). The Quantum counterpart of the Jensen-Shannon divergence (QJSD) between density matrices ρ and σ is defined as $D_{JS}(\rho, \sigma) = S\left(\frac{\rho + \sigma}{2}\right) - \frac{1}{2}(S(\rho) + S(\sigma))$, where $S(\cdot)$ is von Neumann's entropy. QJSD is everywhere defined, bounded, symmetric, and positive if $\rho \neq \sigma$ (Sra, 2021). Similar to the kernel-based entropy, we let the covariance operators play the role of the density matrices to derive a measure of divergence that can be computed directly from data samples.

Definition 2. *Let \mathbb{P} and \mathbb{Q} be two probability measures defined on a measurable space $\{\mathcal{X}, \mathbf{B}_{\mathcal{X}}\}$, and let $\phi : \mathcal{X} \rightarrow \mathcal{H}$ be a mapping to a reproducing kernel Hilbert space (RKHS) \mathcal{H} , such that $\langle \phi(x), \phi(x) \rangle_{\mathcal{H}} = 1$ for all $x \in \mathcal{X}$. Then, the **representation Jensen-Shannon divergence (RJSD)** between uncentered covariance operators $C_{\mathbb{P}}$ and $C_{\mathbb{Q}}$ is defined as:*

$$D_{JS}^\phi(C_{\mathbb{P}}, C_{\mathbb{Q}}) = S\left(\frac{C_{\mathbb{P}} + C_{\mathbb{Q}}}{2}\right) - \frac{1}{2}(S(C_{\mathbb{P}}) + S(C_{\mathbb{Q}})). \quad (9)$$

3.1 Theoretical Properties

RJSD inherits most of the properties of classical and quantum Jensen-Shannon divergence. *Non-negativity:* $D_{JS}^\phi(C_{\mathbb{P}}, C_{\mathbb{Q}}) \geq 0$. *Positivity:* $D_{JS}^\phi(C_{\mathbb{P}}, C_{\mathbb{Q}}) = 0$ if and only if $C_{\mathbb{P}} = C_{\mathbb{Q}}$. *Symmetry:* $D_{JS}^\phi(C_{\mathbb{P}}, C_{\mathbb{Q}}) = D_{JS}^\phi(C_{\mathbb{Q}}, C_{\mathbb{P}})$. *Boundedness:* $D_{JS}^\phi(C_{\mathbb{P}}, C_{\mathbb{Q}}) \leq \log(2)$. Also, $D_{JS}^\phi(C_{\mathbb{P}}, C_{\mathbb{Q}})^{\frac{1}{2}}$ is a metric on the cone of uncentered covariance matrices in any dimension (Virosztek, 2021).

Below, we introduce key properties of RJSD and the connection with its classical counterpart.

Theorem 3. *For all probability measures \mathbb{P} and \mathbb{Q} defined on \mathcal{X} , and covariance operators $C_{\mathbb{P}}$ and $C_{\mathbb{Q}}$ with RKHS mapping $\phi(\cdot)$ under the conditions of Definition 2, the following inequality holds:*

$$D_{JS}^\phi(C_{\mathbb{P}}, C_{\mathbb{Q}}) \leq D_{JS}(\mathbb{P}, \mathbb{Q}) \quad (10)$$

Proof: See Appendix A.3.

Theorem 4. *Let \mathbb{P} and \mathbb{Q} be two probability measures defined on \mathcal{X} . If there exists a mapping ϕ^* such that $\mathbb{P}(x) = \frac{1}{h_{\mathbb{P}}} \langle \phi^*(x) | C_{\mathbb{P}} | \phi^*(x) \rangle$ and $\mathbb{Q}(x) = \frac{1}{h_{\mathbb{Q}}} \langle \phi^*(x) | C_{\mathbb{Q}} | \phi^*(x) \rangle$, then:*

$$D_{JS}(\mathbb{P}, \mathbb{Q}) = D_{JS}^{\phi^*}(C_{\mathbb{P}}, C_{\mathbb{Q}}). \quad (11)$$

Proof: See Appendix A.4.

This theorem implies that the bound in Eqn. 10 is tight for optimal functions $\phi(x)$ that approximate the true underlying distributions through Eqn. 5. Theorems 3 and 4 can be used to obtain a variational estimator of Jensen-Shannon divergence (see Section 4).

Finally, we show that RJSD relates to MMD with kernel $\kappa^2(\cdot, \cdot)$.

Theorem 5. *For all probability measures \mathbb{P} and \mathbb{Q} defined on \mathcal{X} , and covariance operators $C_{\mathbb{P}}$ and $C_{\mathbb{Q}}$ with RKHS mapping $\phi(x)$ such that $\forall x \in \mathcal{X}, \langle \phi(x), \phi(x) \rangle_{\mathcal{H}} = 1$:*

$$D_{JS}(C_{\mathbb{P}}, C_{\mathbb{Q}}) \geq \frac{1}{8} \|C_{\mathbb{P}} - C_{\mathbb{Q}}\|_*^2 \geq \frac{1}{8} \|C_{\mathbb{P}} - C_{\mathbb{Q}}\|_{HS}^2 = \frac{1}{8} \text{MMD}_{\kappa^2}(\mathbb{P}, \mathbb{Q}) \quad (12)$$

Proof: See Appendix A.5.

From this result we should expect RJSD to be at least as efficient as MMD for identifying discrepancies between distributions and that for a characteristic kernel κ , RJSD to be non zero if $\mathbb{P} \neq \mathbb{Q}$.

3.2 Estimating the representation Jensen-Shannon divergence

Given two sets of samples $\mathbf{X} = \{x_i\}_{i=1}^N \subset \mathcal{X}^d$ and $\mathbf{Y} = \{y_i\}_{i=1}^M \subset \mathcal{X}^d$ with unknown distributions \mathbb{P} and \mathbb{Q} , we propose two estimators of RJSD.

Covariance-based estimator: We propose to use Fourier features to construct a mapping function $\phi_{\omega} : \mathcal{X}^d \rightarrow \mathcal{H}^D$ to a finite dimensional RKHS as explained in Section 2.2. Let $\Phi_{\mathbf{X}} \in \mathbb{R}^{N \times D}$ and $\Phi_{\mathbf{Y}} \in \mathbb{R}^{M \times D}$ be the matrices containing the mapped samples of each distribution. Then, the empirical uncentered covariance matrices are computed as $\mathbf{C}_{\mathbf{X}} = \frac{1}{N} \Phi_{\mathbf{X}}^{\top} \Phi_{\mathbf{X}}$ and $\mathbf{C}_{\mathbf{Y}} = \frac{1}{M} \Phi_{\mathbf{Y}}^{\top} \Phi_{\mathbf{Y}}$. Finally, the covariance-based RJSD estimator is defined as:

$$D_{JS}^{\omega}(\mathbf{C}_{\mathbf{X}}, \mathbf{C}_{\mathbf{Y}}) = S(\pi_1 \mathbf{C}_{\mathbf{X}} + \pi_2 \mathbf{C}_{\mathbf{Y}}) - (\pi_1 S(\mathbf{C}_{\mathbf{X}}) + \pi_2 S(\mathbf{C}_{\mathbf{Y}})), \quad (13)$$

where $\pi_1 = \frac{N}{N+M}$ and $\pi_2 = \frac{M}{N+M}$ are the sample proportions of each distribution (e.g. $\frac{1}{2}$ if the samples are balanced). Finally, we use Eqn. 4 to estimate the entropies of the covariance matrices.

This procedure serves a dual purpose: It provides an explicit mapping to the RKHS to construct the empirical covariance matrices essential to compute RJSD. Additionally, it allows a parameterization of the RKHS yielding a kernel-learning strategy. Namely, we can optimize the Fourier features to maximize the divergence between distributions.

Kernel-based estimator: Here, we propose an estimator of RJSD from kernel matrices without an explicit mapping to the RKHS.

Lemma 1. *Let \mathbf{Z} be the mixture of the samples of \mathbf{X} and \mathbf{Y} , that is, $\mathbf{Z} = \{\mathbf{z}_i\}_{i=1}^{N+M}$ where $\mathbf{z}_i = \mathbf{x}_i$ for $i \in \{1, \dots, N\}$ and $\mathbf{z}_i = \mathbf{y}_{i-N}$ for $i \in \{N+1, \dots, N+M\}$. Also, let $\mathbf{K}_{\mathbf{Z}}$ be the kernel matrix consisting of all normalized pairwise kernel evaluations of the samples in \mathbf{Z} , then $S(\pi_1 \mathbf{C}_{\mathbf{X}} + \pi_2 \mathbf{C}_{\mathbf{Y}}) = S(\mathbf{K}_{\mathbf{Z}})$ (Proof: See Appendix A.6).*

Since the spectrum of $\mathbf{K}_{\mathbf{X}}$ and $\mathbf{C}_{\mathbf{X}}$ have the same non-zero eigenvalues, likewise $\mathbf{K}_{\mathbf{Y}}$ and $\mathbf{C}_{\mathbf{Y}}$, the divergence can be directly computed from samples in the input space as:

$$D_{JS}^{\kappa}(\mathbf{X}, \mathbf{Y}) = S(\mathbf{K}_{\mathbf{Z}}) - (\pi_1 S(\mathbf{K}_{\mathbf{X}}) + \pi_2 S(\mathbf{K}_{\mathbf{Y}})) \quad (14)$$

4 Variational Estimation of classical Jensen-Shannon divergence

We exploit the lower bound in Theorem 3 to derive a variational method for estimating the classical Jensen-Shannon divergence (JSD) given only samples from \mathbb{P} and \mathbb{Q} . Accordingly, we choose Φ to be the family of functions $\phi_{\omega} : \mathcal{X}^d \rightarrow \mathcal{H}^D$ parameterized by $\omega \in \Omega$. Here, we aim to optimize the Fourier features to maximize the lower bound in Eqn. 3. Notice that we can also use a neural network f_{ω} with a Fourier features mapping ϕ_{ω} in the last layer, that is, $\phi_{\omega} \circ f_{\omega} = \phi_{\omega}(f_{\omega}(x))$. We call this network a *Fourier-features network (FFN)*. Finally, we can compute the divergence based on this representation, leading to a neural estimator of classical JSD.

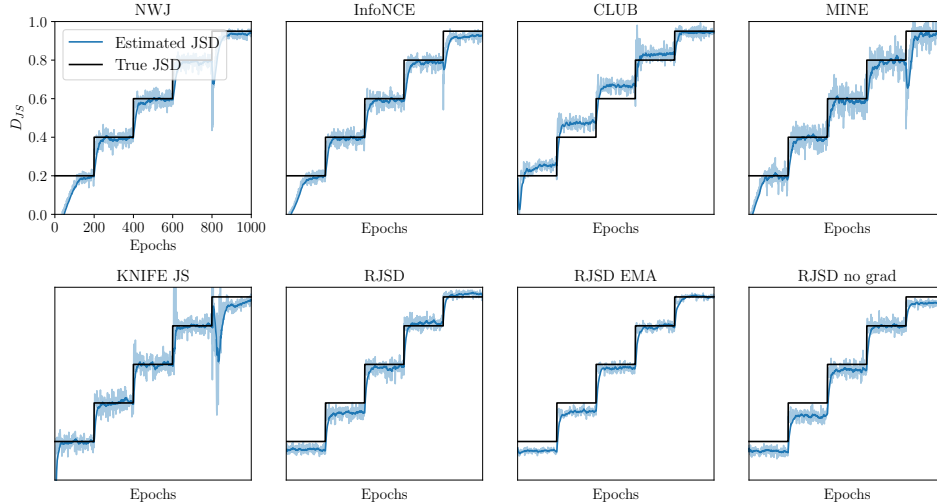


Figure 1: Jensen-Shannon Divergence estimation for two set of samples following Cauchy distributions ($N = 512$). We compare the following estimators: NWJ (Nguyen et al., 2010), infoNCE (Oord et al., 2018), CLUB (Cheng et al., 2020), MINE (Belghazi et al., 2018), KNIFE (Pichler et al., 2022), RJSJ, RJSJ with EMA, RJSJ for a fixed kernel.

Definition 3. (*Jensen-Shannon divergence variational estimator*). Let $\Phi = \{\phi_\omega \circ f_\omega\}_{\omega \in \Omega}$ be the set of functions parameterized by a FFN. We define our JSD variational estimator as:

$$\widehat{D}_{JS}(\mathbb{P}, \mathbb{Q}) = \sup_{\omega \in \Omega} D_{JS}^\omega(C_{\mathbb{P}}, C_{\mathbb{Q}}). \quad (15)$$

This approach leverages the expressive power of deep networks and combines it with the capacity of kernels to embed distributions in a RKHS. This formulation allows to model distributions with complex structures and improve the convergence of the estimator by the universal approximation properties of the neural networks (Wilson et al., 2016; Liu et al., 2020). Algorithm 1 in Appendix B describes the proposed estimator.

5 Experiments

5.1 Variational Jensen-Shannon divergence estimation

First, we evaluate the performance of our variational estimator of Jensen-Shannon divergence (JSD) in a tractable toy experiment. Here, $\mathbb{P} \sim p(x; l_p, s_p)$ and $\mathbb{Q} \sim p(x; l_q, s_q)$ are two Cauchy distributions with location parameters l_p and l_q and scale parameters $s_p = s_q = 1$. We vary the location parameter of \mathbb{Q} over time to control the target divergence. We use a closed form of the JSD between Cauchy distributions derived by Nielsen & Okamura (2022) to determine the location parameter (see Appendix C.1 for more details). Then, we apply Algorithm 1 to estimate JSD drawing $N = 512$ samples from both distributions at every epoch. We compare the estimates of divergence against different neural estimators. JSD corresponds to the mutual information between the mixture distribution and a Bernoulli distribution indicating when a sample is drawn from \mathbb{P} or \mathbb{Q} . Therefore, we use mutual information estimators to approach the JSD estimation, such as NWJ (Nguyen et al., 2010), infoNCE (Oord et al., 2018), CLUB (Cheng et al., 2020), MINE (Belghazi et al., 2018). We also employ KNIFE (Pichler et al., 2022) to estimate the entropy terms and compute JSD.

Fig. 1 shows the estimation results. All compared methods approximate JSD; however, some of them struggle to adapt to distribution changes. These abrupt adjustments could lead to instabilities during training. In contrast to the compared methods, the RJSJ estimator accurately estimates divergence with a lower variance, adjusting itself smoothly to changes in the distributions. Additionally, by using Exponential Moving averages (EMA) of the covariance matrices, the estimation variance decreases further yielding a smoother estimation. Finally, we compute RJSJ for a fixed set of Fourier features without any optimization (no gradients backpropagated), and we can observe that RJSJ still

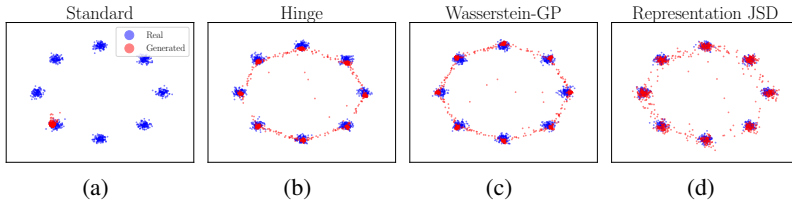


Figure 2: GANs with different loss functions to evaluate mode collapse in eightGaussians dataset. RJSD improves mode coverage and sample diversity.

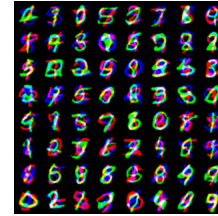


Figure 3: Generated samples using rep JSD.

approximates the true divergence. This result agrees with theorem 4 suggesting that the computed kernel implicitly approximates the underlying distributions of the data.

5.2 Generative Adversarial Networks

Generative Adversarial Networks (GANs) are a family of models to generate images/audio. GANs algorithms minimize the dissimilarity between the generated and the real data distributions (Farnia & Ozdaglar, 2020). For example, the vanilla GAN algorithm (Goodfellow et al., 2020) minimizes the Jensen-Shannon divergence (JSD), whereas Wasserstein-GANs (Arjovsky et al., 2017) and MMD-GANs (Li et al., 2017) minimize their respective statistical distances.

GANs, however, usually suffer from mode collapse failing to cover the multiple modes (classes) of the real data (Choi & Han, 2022). This deficiency yields generative distributions with lower entropy compared to the target distribution (Che et al., 2016). One common approach to prevent mode collapse is through entropy regularizers (Belghazi et al., 2018; Dieng et al., 2019).

Below, we propose a methodology for training GANs using RJSD in the objective function. From first principles, RJSD should work for reducing mode collapse without requiring auxiliary entropy regularizers. The RJSD-GAN is formulated as follows:

$$\min_{\theta \in \Theta} \max_{\omega \in \Omega} D_{JS}^{\omega}(\mathbf{X}, \mathbf{Y}^{\theta}), \quad (16)$$

where \mathbf{X} are samples from the real data, and \mathbf{Y}^{θ} are samples created by a generator G_{θ} . Instead of classifying real and fake samples, we use a *Fourier-features network* $\{\phi_{\omega} \circ f_{\omega}\}_{\omega \in \Omega}$ (FFN, see Section 4) to learn a multidimensional representation in an RKHS where the divergence is maximized. Subsequently, the generator $\{G_{\theta}\}_{\theta \in \Theta}$ attempts to minimize RJSD. We follow a single-step alternating gradient method (see Algorithm 3 in Appendix B). We assess our GAN formulation in two well-known mode-collapse experiments: eight Gaussians dataset and stacked MNIST.

5.2.1 Synthetic experiments

We apply RJSD to train a GAN in a synthetic experiment. The target distribution is a mixture of eight Gaussian distributions arranged in a circle. Fig. 2 shows the real data and the samples generated by various learning functions to train GANs. As expected, the standard (vanilla) GAN fails to generate samples from all modes (Fig. 2(a)). The Hinge (Lim & Ye, 2017) and Wasserstein-GP GANs (Gulrajani et al., 2017) successfully produce samples representing all eight modes, yet Figs. 2(b) and 2(c) exhibit generated samples with reduced variance/diversity (lower entropy) within each mode: a phenomenon termed intra-class collapse. As we observe, the generated samples fail to cover the entire support of each Gaussian mode clustering towards the center. In contrast to the compared methods, the samples generated by the RJSD-GAN show improved mode coverage and higher diversity. This is visually noticeable in Fig. 2(d). Additionally,

Table 1: KL divergence between real and generated distributions on eightmodes dataset.

	Average KL divergence		
	RJSD	Wasserstein-GP	Hinge
	0.699 ± 0.245	0.981 ± 0.701	1.623 ± 1.000

Table 2: Number of modes and KL divergence between real and generated distributions on stacked MNIST.

	Modes (Max 1000)	KL
DCGAN (Radford et al., 2015)	99.0	3.40
ALI (Dumoulin et al., 2016)	16.0	5.40
Unrolled GAN (Metz et al., 2016)	48.7	4.32
VEEGAN (Srivastava et al., 2017)	150	2.95
WGAN-GP (Gulrajani et al., 2017)	959.0	0.72
PresGAN (Dieng et al., 2019)	999.6 ± 0.4	0.11 ± 7.0e-2
PacGAN (Lin et al., 2018)	1000.0 ± 0	0.06 ± 1.0e-2
GAN+MINE (Belghazi et al., 2018)	1000.0 ± 0	0.05 ± 6.9e-3
GAN + rep JSD	1000.0 ± 0	0.04 ± 1.2e-3

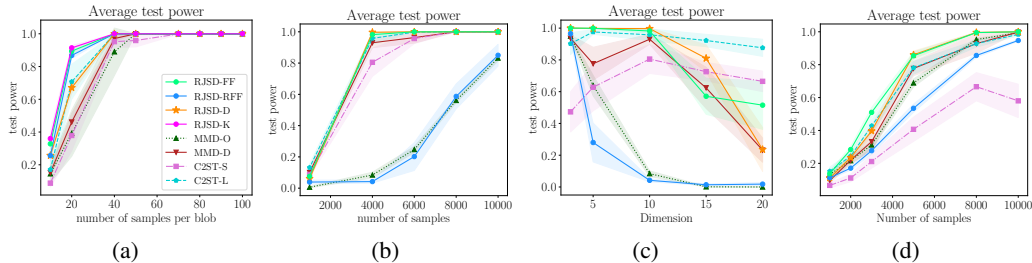


Figure 4: Average test power ($\alpha = 0.05$) over 10 trials on the (a) Blobs dataset. (b) High dimensional Gaussian mixture, fixed $d = 10$. (c) High dimensional Gaussian mixture, fixed $N + M = 4000$ (d) Higgs dataset

we perform the following quantitative analysis. We cluster the eight modes generated by each method and estimate their mean and covariance matrices (see Fig. 5 in Appendix C.2.1). Then, we calculate the Kullback-Leibler (KL) divergence between the real Gaussian modes and their generated counterparts. Finally, we average the divergence among the eight modes. Table 1 highlights the superiority of RJSD in terms of KL divergence when contrasted with the baseline methods. This empirical evidence supports the efficacy of RJSD to avoid mode collapse and to generate samples matching the target distribution beyond visual comparability.

5.2.2 Stacked MNIST

We conduct a quantitative evaluation to assess the efficacy of RJSD in reducing mode collapse on the stacked MNIST dataset. This dataset consists of three randomly sampled MNIST digits stacked along different color channels. This procedure results in 1000 possible classes (modes) corresponding to all combinations of the 10 digits. We use the standard DCGAN generator architecture (Radford et al., 2015), and modify the discriminator architecture to include a Fourier-features mapping (see implementation details in Appendix C.2.2). We compare our method against a considerable number of GAN algorithms using the same generator and following the same evaluation protocol. We utilize a pre-trained classifier to quantify the number of distinct generated modes. Additionally, we calculate the Kullback-Leibler (KL) divergence between the distribution of the generated modes and the real mode distribution. Finally, we average the results over five runs. Table 2 shows the results, and RJSD captures all modes and steadily generates samples from all classes achieving the lowest KL-divergence compared to the baseline approaches. Although our algorithm is a standard GAN that explicitly minimizes the Jensen-Shannon divergence, RJSD does not require the incorporation of entropy regularizers or mode-collapse prevention mechanisms beyond the learning function itself.

5.3 Two sample testing

We evaluate the performance of the proposed divergence for two-sample testing on different datasets and compare it against different state-of-the-art (SOTA) methods. We perform the following tests: (a) RJSD-FF: Two-sample test based on RJSD, optimizing the Fourier features applied to the input data. (b) RJSD-RFF: Two-sample test based on RJSD using random Fourier features, optimizing just the length-scale of the associated Gaussian kernel. (c) RJSD-D: Two-sample test based on RJSD using a deep Fourier-features network as explained in section 4 (see implementation details in Appendix C.3). (d) RJSD-K¹: Two-sample test based on the kernel RJSD estimator, optimizing the length-scale of a Gaussian kernel. (e) MMD-O: Two-sample test based on MMD, optimizing the length-scale of the Gaussian kernel (Liu et al., 2020). (f) MMD-D: Two-sample test based on MMD with a deep kernel (Liu et al., 2020). (g) C2ST-L: a classifier two-sample test based on the output classification scores (Cheng & Cloninger, 2022). (h) C2ST-S: a classifier two-sample test based on the sign of the output classification scores (Lopez-Paz & Oquab, 2016).

We perform two-sample testing on two synthetic and two real-world datasets. The testing procedure is detailed in Appendix C.3.

¹We did not perform this test for large size datasets due to computational restrictions

Table 3: MNIST average test power ($\alpha = 0.05$). Bold represents higher mean per column.

$N + M$	200	300	400	500	600
RJSD-FF	0.374 ± 0.100	0.811 ± 0.012	0.996 ± 0.001	1.000 ± 0.000	1.000 ± 0.000
RJSD-RFF	0.184 ± 0.025	0.320 ± 0.029	0.436 ± 0.030	0.644 ± 0.037	0.800 ± 0.051
RJSD-D	0.352 ± 0.084	0.898 ± 0.108	1.000 ± 0.000	1.000 ± 0.000	1.000 ± 0.000
MMD-O	0.148 ± 0.035	0.221 ± 0.042	0.283 ± 0.042	0.398 ± 0.050	0.498 ± 0.035
MMD-D	0.449 ± 0.124	0.704 ± 0.182	0.985 ± 0.010	0.999 ± 0.003	1.000 ± 0.000
C2ST-L	0.254 ± 0.126	0.424 ± 0.113	0.818 ± 0.102	0.967 ± 0.029	0.994 ± 0.010
C2ST-S	0.181 ± 0.112	0.364 ± 0.104	0.759 ± 0.121	0.945 ± 0.042	0.986 ± 0.014

Blobs dataset (Liu et al., 2020): In this dataset, \mathbb{P} and \mathbb{Q} are mixtures of nine Gaussians with the same modes. Each mode in \mathbb{P} is an isotropic Gaussian; however, the modes in \mathbb{Q} have different covariances. Here, we perform two-sample testing increasing the number of samples per blob ($N = 9 \times$ samples per blob). Fig 4(a) presents the results. We can clearly see that RJSD-FF, RJSD-D, and JSD outperform all SOTA methods. We can conclude that even for a small number of samples the RJSD-based methods exhibit high test power.

High-Dimensional Gaussian Mixtures (Liu et al., 2020): We assess the performance of RJSD at high dimensions on a bimodal multidimensional Gaussian dataset. In this dataset, \mathbb{P} and \mathbb{Q} have the same modes, and their covariances differ only on a single dimension. See Liu et al. (2020) for details. We test both, changing the number of samples while keeping the dimension constant ($d = 10$) and maintaining the number of samples ($N = 4000$) while modifying the dimensionality. Figs. 4(b) and 4(c) display the results. RJSD-D and RJSD-FF are the winners in most settings, although C2ST-L performs better at higher dimensions.

Higgs dataset (Baldi et al., 2014): Following Liu et al. (2020) we perform two-sample testing on the Higgs dataset ($d = 4$) as we increase the number of samples. Fig. 4(d) shows the results. Once again, RJSD-D and RJSD-FF outperform the baselines in almost all scenarios.

MNIST generative model: Here, we train RJSD models to distinguish between the distribution \mathbb{P} of MNIST digits and the distribution \mathbb{Q} of generated samples from a pretrained deep convolutional generative adversarial network (DCGAN) (Radford et al., 2015). Table 3 reports the average test power for all methods as we increase the number of samples. RJSD-D consistently outperforms the compared methods, except with the lowest number of observations.

6 Conclusions

We introduce the representation Jensen-Shannon divergence (RJSD), a novel measure based on embedding distributions in a feature space allowing the construction of non-parametric estimators based on Fourier features. Notably, this estimator demonstrates scalability, differentiability, making it suitable for diverse machine-learning problems. We demonstrated that RJSD provides a lower bound on the classical Jensen-Shannon divergence leading to a variational estimator of high precision compared to related approaches. We leveraged this novel divergence to train generative networks, and the empirical results show that RJSD effectively mitigates mode collapse yielding generative models that produce more accurate and diverse results. Furthermore, when applied to two-sample testing, RJSD surpassed other SOTA techniques demonstrating superior performance and reliability to discriminate between distributions. These findings highlight the significant practical implications of our divergence measure.

Acknowledgments

This material is based upon work supported by the Office of the Under Secretary of Defense for Research and Engineering under award number FA9550-21-1-0227.

References

Martin Arjovsky, Soumith Chintala, and Léon Bottou. Wasserstein generative adversarial networks. In *International conference on machine learning*, pp. 214–223. PMLR, 2017.

- Francis Bach. Information theory with kernel methods. *IEEE Transactions on Information Theory*, 2022.
- Pierre Baldi, Peter Sadowski, and Daniel Whiteson. Searching for exotic particles in high-energy physics with deep learning. *Nature communications*, 5(1):4308, 2014.
- Mohamed Ishmael Belghazi, Aristide Baratin, Sai Rajeshwar, Sherjil Ozair, Yoshua Bengio, Aaron Courville, and Devon Hjelm. Mutual information neural estimation. In *International conference on machine learning*, pp. 531–540. PMLR, 2018.
- Thomas B Berrett and Richard J Samworth. Efficient two-sample functional estimation and the super-oracle phenomenon. *arXiv preprint arXiv:1904.09347*, 2019.
- Jop Briët and Peter Harremoës. Properties of classical and quantum jensen-shannon divergence. *Physical review A*, 79(5):052311, 2009.
- Yuheng Bu, Shaofeng Zou, Yingbin Liang, and Venugopal V Veeravalli. Estimation of kl divergence: Optimal minimax rate. *IEEE Transactions on Information Theory*, 64(4):2648–2674, 2018.
- Tong Che, Yanran Li, Athul Paul Jacob, Yoshua Bengio, and Wenjie Li. Mode regularized generative adversarial networks. *arXiv preprint arXiv:1612.02136*, 2016.
- Pengyu Cheng, Weituo Hao, Shuyang Dai, Jiachang Liu, Zhe Gan, and Lawrence Carin. Club: A contrastive log-ratio upper bound of mutual information. In *International conference on machine learning*, pp. 1779–1788. PMLR, 2020.
- Xiuyuan Cheng and Alexander Cloninger. Classification logit two-sample testing by neural networks for differentiating near manifold densities. *IEEE Transactions on Information Theory*, 68(10): 6631–6662, 2022.
- Jinyoung Choi and Bohyung Han. Mcl-gan: Generative adversarial networks with multiple specialized discriminators. *Advances in Neural Information Processing Systems*, 35:29597–29609, 2022.
- Emmanuele DiBenedetto and Emmanuele Debenedetto. *Real analysis*, pp. 156–157. Springer, 2002.
- Adji B Dieng, Francisco JR Ruiz, David M Blei, and Michalis K Titsias. Prescribed generative adversarial networks. *arXiv preprint arXiv:1910.04302*, 2019.
- Yu G Dmitriev and Felix P Tarasenko. On the estimation of functionals of the probability density and its derivatives. *Theory of Probability & Its Applications*, 18(3):628–633, 1974.
- Vincent Dumoulin, Ishmael Belghazi, Ben Poole, Olivier Mastropietro, Alex Lamb, Martin Arjovsky, and Aaron Courville. Adversarially learned inference. *arXiv preprint arXiv:1606.00704*, 2016.
- Farzan Farnia and Asuman Ozdaglar. Gans may have no nash equilibria. *arXiv preprint arXiv:2002.09124*, 2020.
- Fabio A González, Alejandro Gallego, Santiago Toledo-Cortés, and Vladimir Vargas-Calderón. Learning with density matrices and random features. *Quantum Machine Intelligence*, 4(2):23, 2022.
- Ian Goodfellow, Jean Pouget-Abadie, Mehdi Mirza, Bing Xu, David Warde-Farley, Sherjil Ozair, Aaron Courville, and Yoshua Bengio. Generative adversarial networks. *Communications of the ACM*, 63(11):139–144, 2020.
- Arthur Gretton, Karsten M Borgwardt, Malte J Rasch, Bernhard Schölkopf, and Alexander Smola. A kernel two-sample test. *The Journal of Machine Learning Research*, 13(1):723–773, 2012.
- Ishaan Gulrajani, Faruk Ahmed, Martin Arjovsky, Vincent Dumoulin, and Aaron C Courville. Improved training of wasserstein gans. *Advances in neural information processing systems*, 30, 2017.
- Yanjun Han, Jiantao Jiao, Tsachy Weissman, and Yihong Wu. Optimal rates of entropy estimation over lipschitz balls. 2020.

- Jhoan Keider Hoyos Osorio, Oscar Skean, Austin J Brockmeier, and Luis Gonzalo Sanchez Giraldo. The representation jensen-rényi divergence. In *ICASSP 2022-2022 IEEE International Conference on Acoustics, Speech and Signal Processing (ICASSP)*, pp. 4313–4317. IEEE, 2022.
- Akshay Krishnamurthy, Kirthevasan Kandasamy, Barnabas Poczos, and Larry Wasserman. Non-parametric estimation of renyi divergence and friends. In *International Conference on Machine Learning*, pp. 919–927. PMLR, 2014.
- Chun-Liang Li, Wei-Cheng Chang, Yu Cheng, Yiming Yang, and Barnabás Póczos. Mmd gan: Towards deeper understanding of moment matching network. *Advances in neural information processing systems*, 30, 2017.
- Yingzhen Li and Richard E Turner. Rényi divergence variational inference. *Advances in neural information processing systems*, 29, 2016.
- Tengyuan Liang. Estimating certain integral probability metric (ipm) is as hard as estimating under the ipm. *arXiv preprint arXiv:1911.00730*, 2019.
- Jae Hyun Lim and Jong Chul Ye. Geometric gan. *arXiv preprint arXiv:1705.02894*, 2017.
- Zinan Lin, Ashish Khetan, Giulia Fanti, and Sewoong Oh. Pacgan: The power of two samples in generative adversarial networks. *Advances in neural information processing systems*, 31, 2018.
- Feng Liu, Wenkai Xu, Jie Lu, Guangquan Zhang, Arthur Gretton, and Danica J Sutherland. Learning deep kernels for non-parametric two-sample tests. In *International conference on machine learning*, pp. 6316–6326. PMLR, 2020.
- David Lopez-Paz and Maxime Oquab. Revisiting classifier two-sample tests. *arXiv preprint arXiv:1610.06545*, 2016.
- Luke Metz, Ben Poole, David Pfau, and Jascha Sohl-Dickstein. Unrolled generative adversarial networks. *arXiv preprint arXiv:1611.02163*, 2016.
- Kevin Moon and Alfred Hero. Multivariate f-divergence estimation with confidence. *Advances in neural information processing systems*, 27, 2014.
- Kevin R Moon, Kumar Sricharan, Kristjan Greenewald, and Alfred O Hero III. Ensemble estimation of information divergence. *Entropy*, 20(8):560, 2018.
- Krikamol Muandet, Kenji Fukumizu, Bharath Sriperumbudur, Bernhard Schölkopf, et al. Kernel mean embedding of distributions: A review and beyond. *Foundations and Trends® in Machine Learning*, 10(1-2):1–141, 2017.
- Martin Müller-Lennert, Frédéric Dupuis, Oleg Szehr, Serge Fehr, and Marco Tomamichel. On quantum rényi entropies: A new generalization and some properties. *Journal of Mathematical Physics*, 54(12):122203, 2013.
- XuanLong Nguyen, Martin J Wainwright, and Michael I Jordan. Estimating divergence functionals and the likelihood ratio by convex risk minimization. *IEEE Transactions on Information Theory*, 56(11):5847–5861, 2010.
- Frank Nielsen and Kazuki Okamura. On f-divergences between cauchy distributions. *IEEE Transactions on Information Theory*, 2022.
- Morteza Noshad, Kevin R Moon, Salimeh Yasaei Sekeh, and Alfred O Hero. Direct estimation of information divergence using nearest neighbor ratios. In *2017 IEEE International Symposium on Information Theory (ISIT)*, pp. 903–907. IEEE, 2017.
- Aaron van den Oord, Yazhe Li, and Oriol Vinyals. Representation learning with contrastive predictive coding. *arXiv preprint arXiv:1807.03748*, 2018.
- Georg Pichler, Pierre Jean A Colombo, Malik Boudiaf, Günther Koliander, and Pablo Piantanida. A differential entropy estimator for training neural networks. In *International Conference on Machine Learning*, pp. 17691–17715. PMLR, 2022.

- Alec Radford, Luke Metz, and Soumith Chintala. Unsupervised representation learning with deep convolutional generative adversarial networks. *arXiv preprint arXiv:1511.06434*, 2015.
- Ali Rahimi and Benjamin Recht. Random features for large-scale kernel machines. *Advances in neural information processing systems*, 20, 2007.
- Luis Gonzalo Sanchez Giraldo, Murali Rao, and Jose C Principe. Measures of entropy from data using infinitely divisible kernels. *IEEE Transactions on Information Theory*, 61(1):535–548, 2014.
- Shashank Singh and Barnabás Póczos. Generalized exponential concentration inequality for rényi divergence estimation. In *International Conference on Machine Learning*, pp. 333–341. PMLR, 2014.
- Suvrit Sra. Metrics induced by jensen-shannon and related divergences on positive definite matrices. *Linear Algebra and its Applications*, 616:125–138, 2021.
- Sreejith Sreekumar and Ziv Goldfeld. Neural estimation of statistical divergences. *Journal of machine learning research*, 23(126), 2022.
- Bharath K Sriperumbudur, Kenji Fukumizu, Arthur Gretton, Bernhard Schölkopf, and Gert RG Lanckriet. On the empirical estimation of integral probability metrics. 2012.
- Akash Srivastava, Lazar Valkov, Chris Russell, Michael U Gutmann, and Charles Sutton. Veegan: Reducing mode collapse in gans using implicit variational learning. *Advances in neural information processing systems*, 30, 2017.
- Dániel Virosztek. The metric property of the quantum jensen-shannon divergence. *Advances in Mathematics*, 380:107595, 2021.
- Andrew Gordon Wilson, Zhiting Hu, Ruslan Salakhutdinov, and Eric P Xing. Deep kernel learning. In *Artificial intelligence and statistics*, pp. 370–378. PMLR, 2016.
- Yuhong Yang and Andrew Barron. Information-theoretic determination of minimax rates of convergence. *Annals of Statistics*, pp. 1564–1599, 1999.
- Shujian Yu, Luis Gonzalo Sanchez Giraldo, Robert Jenssen, and Jose C Principe. Multivariate extension of matrix-based rényi’s α -order entropy functional. *IEEE transactions on pattern analysis and machine intelligence*, 42(11):2960–2966, 2019.
- Shujian Yu, Francesco Alesiani, Xi Yu, Robert Jenssen, and Jose Principe. Measuring dependence with matrix-based entropy functional. In *Proceedings of the AAAI Conference on Artificial Intelligence*, volume 35, pp. 10781–10789, 2021.

Appendix

Next, we present the proofs of the theorems and properties described in the paper. Additionally, we include implementation details for all the experiments reported. All the codes to reproduce the results in the paper can be found in the following anonymous Github repository: <https://github.com/uk-cliplab/representationJSD>.

A Proofs of theorems

A.1 Proof Theorem 1

Proof.

$$\begin{aligned}
H(\mathbb{P}, \mathbb{P}_\phi) &= - \int_{\mathcal{X}} \log [\mathbb{P}_\phi(x)] d\mathbb{P}(x) \\
&= - \int_{\mathcal{X}} \log \left[\frac{1}{h} \langle \phi(x) | C_{\mathbb{P}} | \phi(x) \rangle \right] d\mathbb{P}(x) \\
&= - \int_{\mathcal{X}} \sum_{i=1}^{N_{\mathcal{J}\mathcal{C}}} \langle \phi(x) | u_i \rangle \log(\lambda_i) \langle u_i | \phi(x) \rangle d\mathbb{P}(x) + \int_{\mathcal{X}} \log(h) d\mathbb{P}(x) \\
&= - \int_{\mathcal{X}} \sum_{i=1}^{N_{\mathcal{J}\mathcal{C}}} \log(\lambda_i) \langle \phi(x) | u_i \rangle \langle u_i | \phi(x) \rangle d\mathbb{P}(x) + \log(h).
\end{aligned}$$

Notice that $\langle \phi(x) | u_i \rangle \langle u_i | \phi(x) \rangle$ corresponds to the squared of the inner product between $\phi(x)$ and u_i , where the u_i 's are the eigenfunctions of $C_{\mathbb{P}}$. Therefore, the quantity $-\log(\lambda_i) \langle \phi(x) | u_i \rangle \langle u_i | \phi(x) \rangle$ is always positive. Thus, we can apply Tonelli's theorem (DiBenedetto & DeBenedetto, 2002) to take the sum out of the integral:

$$\begin{aligned}
H(\mathbb{P}, \mathbb{P}_\phi) &= - \sum_{i=1}^{N_{\mathcal{J}\mathcal{C}}} \log(\lambda_i) \int_{\mathcal{X}} \langle \phi(x) | u_i \rangle \langle u_i | \phi(x) \rangle d\mathbb{P}(x) + \log(h) \\
&= - \sum_{i=1}^{N_{\mathcal{J}\mathcal{C}}} \log(\lambda_i) \int_{\mathcal{X}} \langle u_i | \phi(x) \rangle \langle \phi(x) | u_i \rangle d\mathbb{P}(x) + \log(h) \\
&= - \sum_{i=1}^{N_{\mathcal{J}\mathcal{C}}} \log(\lambda_i) \int_{\mathcal{X}} \langle u_i | \phi(x) \otimes \phi(x) | u_i \rangle d\mathbb{P}(x) + \log(h) \\
&= - \sum_{i=1}^{N_{\mathcal{J}\mathcal{C}}} \log(\lambda_i) \left\langle u_i \left| \int_{\mathcal{X}} \phi(x) \otimes \phi(x) d\mathbb{P}(x) \right| u_i \right\rangle + \log(h) \\
&= - \sum_{i=1}^{N_{\mathcal{J}\mathcal{C}}} \log(\lambda_i) \langle u_i | C_{\mathbb{P}} | u_i \rangle + \log(h) \\
&= - \sum_{i=1}^{N_{\mathcal{J}\mathcal{C}}} \lambda_i \log \lambda_i + \log(h) \\
&= S(C_{\mathbb{P}}) + \log(h)
\end{aligned}$$

□

A.2 Proof Theorem 2

We approach the convergence problem from a perspective of density estimation. We start by proving the following lemma:

Lemma 2. *Let $\hat{\mathbb{P}}_\gamma(x)$ be the empirical kernel density function by a Gaussian kernel with scale parameter γ . Similarly, let $\hat{\mathbb{P}}_\omega(x)$ be the kernel density function by a Fourier feature mapping*

approximating the Gaussian kernel with scale parameter $\frac{\gamma}{2}$, then

$$\sup_{x \in \mathcal{X}} |\hat{\mathbb{P}}_\gamma(x) - \hat{\mathbb{P}}_\omega(x)| \leq \epsilon, \quad (17)$$

with probability at least $1 - 2^8 \left(\frac{\sqrt{d}\gamma h_\gamma \text{diam}(\mathcal{X})}{2\epsilon} \right)^2 \exp\left(\frac{-D\epsilon^2}{h_\gamma^2(d+2)}\right)$

Proof. We follow a similar proof as González et al. (2022) with some revised results.

$$\hat{\mathbb{P}}_\gamma(x) = \frac{1}{h_\gamma N} \sum_{i=1}^N \left(\exp\left(-\frac{\gamma \|x - x_i\|^2}{2}\right) \right)^2 = \frac{1}{h_\gamma N} \sum_{i=1}^N \exp(-\gamma \|x - x_i\|^2)$$

Similarly,

$$\begin{aligned} \hat{\mathbb{P}}_\omega(x) &= \frac{1}{h_\gamma} \phi_\omega(x) \mathbf{C}_X \phi_\omega^\top(x) = \frac{1}{h_\gamma} \phi_\omega(x) \left(\frac{1}{N} \sum_{i=1}^N \phi_\omega(x_i)^\top \phi_\omega(x_i) \right) \phi_\omega^\top(x) \\ &= \frac{1}{h_\gamma N} \sum_{i=1}^N \phi_\omega(x) \phi_\omega(x_i)^\top \phi_\omega(x_i) \phi_\omega^\top(x) = \frac{1}{h_\gamma N} \sum_{i=1}^N (\phi_\omega(x) \phi_\omega(x_i)^\top)^2 \end{aligned}$$

Now, by Claim 1 by Rahimi & Recht (2007) we have that for a Gaussian kernel with parameter $\frac{\gamma}{2}$:

$$\sup_{x, x' \in \mathcal{X}} \left| \phi_\omega(x) \phi_\omega(x')^\top - \exp\left(-\frac{\gamma \|x - x'\|^2}{2}\right) \right| \leq \epsilon,$$

with probability at least $1 - 2^8 \left(\frac{\sqrt{d}\gamma \text{diam}(\mathcal{X})}{\epsilon} \right)^2 \exp\left(\frac{-D\epsilon^2}{4(d+2)}\right) = 1 - B$.

Next, we use this result to bound the difference between the probability distributions.

$$\begin{aligned} \sup_{x \in \mathcal{X}} \left| \hat{\mathbb{P}}_\gamma(x) - \hat{\mathbb{P}}_\omega(x) \right| &= \sup_{x \in \mathcal{X}} \left| \frac{1}{h_\gamma N} \sum_{i=1}^N \exp(-\gamma \|x - x_i\|^2) - (\phi_\omega(x) \phi_\omega(x_i)^\top)^2 \right| \\ &\leq \frac{1}{h_\gamma N} \sum_{i=1}^N \sup_{x \in \mathcal{X}} \left| \exp(-\gamma \|x - x_i\|^2) - (\phi_\omega(x) \phi_\omega(x_i)^\top)^2 \right| \end{aligned}$$

Notice that

$$\begin{aligned} &\left| \exp(-\gamma \|x - x_i\|^2) - (\phi_\omega(x) \phi_\omega(x_i)^\top)^2 \right| \leq \\ &\left| \exp\left(-\frac{\gamma \|x - x_i\|^2}{2}\right) - \phi_\omega(x) \phi_\omega(x_i)^\top \right| \left| \exp\left(-\frac{\gamma \|x - x_i\|^2}{2}\right) + \phi_\omega(x) \phi_\omega(x_i)^\top \right| \\ &\leq 2 \left| \exp\left(-\frac{\gamma \|x - x_i\|^2}{2}\right) - \phi_\omega(x) \phi_\omega(x_i)^\top \right| \end{aligned}$$

Therefore,

$$\begin{aligned} \sup_{x \in \mathcal{X}} \left| \hat{\mathbb{P}}_\gamma(x) - \hat{\mathbb{P}}_\omega(x) \right| &\leq \frac{2}{h_\gamma N} \sum_{i=1}^N \sup_{x \in \mathcal{X}} \left| \exp\left(-\frac{\gamma \|x - x_i\|^2}{2}\right) - \phi_\omega(x) \phi_\omega(x_i)^\top \right| \\ &\leq \frac{2}{h_\gamma N} \sum_{i=1}^N \epsilon = \frac{2\epsilon}{h_\gamma}, \end{aligned}$$

with probability at least $1 - B$. Redefining $\epsilon = \frac{2\epsilon}{h_\gamma}$ and plugging this value in the probability we obtain the desired result. \square

Next, we use Schuster's Lemma (Dmitriev & Tarasenko, 1974) which proves that a Gaussian kernel density estimator can approximate any bounded distribution, and that there exists constants C_1 and C_2 such that

$$\sup_{x \in \mathcal{X}} \left| \hat{\mathbb{P}}_\gamma(x) - \mathbb{P}(x) \right| < \epsilon, \quad (18)$$

with probability at least $1 - C_1 \exp\left(\frac{-C_2 N \epsilon^2}{2\gamma}\right)$, where $\gamma = \frac{1}{2\sigma_N^2}$ and $\sigma_N = \mathcal{O}(\epsilon)$ with $\sigma_N \rightarrow 0$ as $N \rightarrow \infty$.

Combining Eqns. 17 and 18, using $\frac{\epsilon}{2}$, we obtain by applying triangle inequality that:

$$\sup_{x \in \mathcal{X}} \left| \hat{\mathbb{P}}_\omega(x) - \mathbb{P}(x) \right| < \left| \hat{\mathbb{P}}_\omega(x) - \hat{\mathbb{P}}_\gamma(x) \right| + \left| \hat{\mathbb{P}}_\gamma(x) - \mathbb{P}(x) \right| \epsilon < \frac{\epsilon}{2} + \frac{\epsilon}{2} = \epsilon,$$

with probability $1 - \max\{P_3(N; \epsilon), P_2(D; \epsilon)\}$ where $P_3(N; \epsilon) = 1 - C_1 \exp\left(-\frac{C_2 N \epsilon^2}{4\gamma}\right)$, and $P_2(D; \epsilon) = 2^8 \left(\frac{\sqrt{d\gamma} h_\gamma \text{diam}(\mathcal{X})}{\epsilon}\right)^2 \exp\left(\frac{-D\epsilon^2}{h_\gamma^2(d+2)}\right)$.

Finally, we can adapt Theorem 2 by Dmitriev & Tarasenko (1974) to show the convergence of the entropy induced by the Fourier features as follows:

$$\Pr \left\{ |H(\mathbb{P}) - H(\hat{\mathbb{P}}_\omega)| < \epsilon \right\} > 1 - \max\{P_1(N; \epsilon), P_2(D; \epsilon)\}, \quad (19)$$

where $P_1(N; \epsilon) = C_1 \exp\left(-\frac{C_2}{16} \epsilon^2 N^{\frac{1}{10}}\right)$, and $P_2(D; \epsilon) = 2^8 \left(\frac{\sqrt{d\gamma} h_\gamma \text{diam}(\mathcal{X})}{\epsilon}\right)^2 \exp\left(\frac{-D\epsilon^2}{h_\gamma^2(d+2)}\right)$.

Finally, following a similar strategy to the proof of Theorem 1, we can conclude that $H(\hat{\mathbb{P}}_\omega) = S(\mathbf{C}_X) + \log(h_\gamma)$, which yields the desired result. \square

A.3 Proof Theorem 3

Proof. For equation 10 we have the following

$$\begin{aligned} D_{JS}^\phi(C_{\mathbb{P}}, C_{\mathbb{Q}}) &= \frac{1}{2} D_{KL}^\phi(C_{\mathbb{P}}, C_{\mathbb{M}}) + \frac{1}{2} D_{KL}^\phi(C_{\mathbb{Q}}, C_{\mathbb{M}}) \\ &= \frac{1}{2} D_{KL}^\phi \left(\int_{\mathcal{X}} \phi(x) \otimes \phi(x) d\mathbb{P}(x) \mid \int_{\mathcal{X}} \phi(x) \otimes \phi(x) d\mathbb{M}(x) \right) + \\ &\quad + \frac{1}{2} D_{KL}^\phi \left(\int_{\mathcal{X}} \phi(x) \otimes \phi(x) d\mathbb{Q}(x) \mid \int_{\mathcal{X}} \phi(x) \otimes \phi(x) d\mathbb{M}(x) \right) \\ &= \frac{1}{2} D_{KL}^\phi \left(\int_{\mathcal{X}} \phi(x) \otimes \phi(x) d\mathbb{P}(x) \mid \int_{\mathcal{X}} \frac{d\mathbb{M}}{d\mathbb{P}}(x) \phi(x) \otimes \phi(x) d\mathbb{P}(x) \right) + \\ &\quad + \frac{1}{2} D_{KL}^\phi \left(\int_{\mathcal{X}} \phi(x) \otimes \phi(x) d\mathbb{Q}(x) \mid \int_{\mathcal{X}} \frac{d\mathbb{M}}{d\mathbb{Q}}(x) \phi(x) \otimes \phi(x) d\mathbb{P}(x) \right). \end{aligned}$$

Since D_{KL}^ϕ is jointly convex (Bach, 2022), then

$$\begin{aligned} D_{JS}^\phi(C_{\mathbb{P}}, C_{\mathbb{Q}}) &\leq \frac{1}{2} \int_{\mathcal{X}} D_{KL}^\phi \left(\phi(x) \otimes \phi(x) \mid \frac{d\mathbb{M}}{d\mathbb{P}}(x) \phi(x) \otimes \phi(x) \right) d\mathbb{P}(x) + \\ &\quad + \frac{1}{2} \int_{\mathcal{X}} D_{KL}^\phi \left(\phi(x) \otimes \phi(x) \mid \frac{d\mathbb{M}}{d\mathbb{Q}}(x) \phi(x) \otimes \phi(x) \right) d\mathbb{Q}(x). \end{aligned}$$

Notice that $\phi(x) \otimes \phi(x)$ is a rank-1 covariance operator with one eigenvalue equal $\|\phi(x)\|^2 = 1$ and one eigen vector $\phi(x)$, therefore, it can be simplified as:

$$\begin{aligned}
D_{JS}^\phi(C_{\mathbb{P}}, C_{\mathbb{Q}}) &\leq \frac{1}{2} \int_{\mathcal{X}} D_{KL}^\phi \left(1 \left| \frac{d\mathbb{M}}{d\mathbb{P}}(x) \right. \right) d\mathbb{P}(x) + \frac{1}{2} \int_{\mathcal{X}} D_{KL}^\phi \left(1 \left| \frac{d\mathbb{M}}{d\mathbb{Q}}(x) \right. \right) d\mathbb{Q}(x) \\
&= \frac{1}{2} \int_{\mathcal{X}} D_{KL}^\phi \left(1 \left| \frac{d\mathbb{M}}{d\mathbb{P}}(x) \right. \right) d\mathbb{P}(x) + \frac{1}{2} \int_{\mathcal{X}} D_{KL}^\phi \left(1 \left| \frac{d\mathbb{M}}{d\mathbb{Q}}(x) \right. \right) d\mathbb{Q}(x) \\
&= \frac{1}{2} \int_{\mathcal{X}} -\log \left(\frac{d\mathbb{M}}{d\mathbb{P}}(x) \right) d\mathbb{P}(x) + \frac{1}{2} \int_{\mathcal{X}} -\log \left(\frac{d\mathbb{M}}{d\mathbb{Q}}(x) \right) d\mathbb{Q}(x) \\
&= \frac{1}{2} D_{KL}(\mathbb{P}, \mathbb{M}) + \frac{1}{2} D_{KL}(\mathbb{Q}, \mathbb{M}) = D_{JS}(\mathbb{P}, \mathbb{Q})
\end{aligned}$$

□

A.4 Proof Theorem 4

Proof. Notice that for Gaussian Kernels, the normalizing constant only depends on the scale parameter γ which is independent of the data, thus $h_{\mathbb{P}} = h_{\mathbb{Q}}$. Hence,

$$\begin{aligned}
H \left(\frac{\mathbb{P} + \mathbb{Q}}{2} \right) &= - \int_{\mathcal{X}} \log \left[\frac{1}{2h} \langle \phi^*(x) | C_{\mathbb{P}} | \phi^*(x) \rangle + \frac{1}{2h} \langle \phi^*(x) | C_{\mathbb{Q}} | \phi^*(x) \rangle \right] d\mathbb{M}(x) \\
&= - \int_{\mathcal{X}} \log \left[\left\langle \phi^*(x) \left| \frac{C_{\mathbb{P}} + C_{\mathbb{Q}}}{2} \right| \phi^*(x) \right\rangle \right] d\mathbb{M}(x) + \log(h) \\
&= S \left(\frac{C_{\mathbb{P}} + C_{\mathbb{Q}}}{2} \right) + \log(h)
\end{aligned}$$

where $\mathbb{M}(x) = \frac{\mathbb{P}(x) + \mathbb{Q}(x)}{2}$. Using the results from theorem 1, it is straightforward to show that

$$\begin{aligned}
D_{JS}(\mathbb{P}, \mathbb{Q}) &= S \left(\frac{C_{\mathbb{P}} + C_{\mathbb{Q}}}{2} \right) - \frac{1}{2} (S(C_{\mathbb{P}}) + S(C_{\mathbb{Q}})) + \log(h) - \frac{1}{2} (\log(h) + \log(h)) \\
&= S \left(\frac{C_{\mathbb{P}} + C_{\mathbb{Q}}}{2} \right) - \frac{1}{2} (S(C_{\mathbb{P}}) + S(C_{\mathbb{Q}})) \\
&= D_{JS}^{\phi^*}(C_{\mathbb{P}}, C_{\mathbb{Q}}).
\end{aligned}$$

□

A.5 Proof Theorem 5

Proof. To prove this theorem, we use (Proposition 4.e) by Bach (2022). We have that

$$D_{KL}^\phi(C_{\mathbb{P}} | C_{\mathbb{Q}}) \geq \frac{1}{2} \|C_{\mathbb{P}} - C_{\mathbb{Q}}\|_*^2 \geq \frac{1}{2} \|C_{\mathbb{P}} - C_{\mathbb{Q}}\|_{\text{HS}}^2$$

Since

$$\begin{aligned}
D_{JS}^\phi(C_{\mathbb{P}}, C_{\mathbb{Q}}) &= \frac{1}{2} D_{KL}^\phi(C_{\mathbb{P}}, C_{\mathbb{M}}) + \frac{1}{2} D_{KL}^\phi(C_{\mathbb{Q}}, C_{\mathbb{M}}) \\
&\geq \frac{1}{4} \left\| C_{\mathbb{P}} - \frac{1}{2}(C_{\mathbb{P}} + C_{\mathbb{Q}}) \right\|_*^2 + \frac{1}{4} \left\| C_{\mathbb{Q}} - \frac{1}{2}(C_{\mathbb{P}} + C_{\mathbb{Q}}) \right\|_*^2 \\
&\geq \frac{1}{4} \left\| \frac{1}{2} C_{\mathbb{P}} - \frac{1}{2} C_{\mathbb{Q}} \right\|_*^2 + \frac{1}{4} \left\| \frac{1}{2} C_{\mathbb{Q}} - \frac{1}{2} C_{\mathbb{P}} \right\|_*^2 = \frac{1}{8} \|C_{\mathbb{P}} - C_{\mathbb{Q}}\|_*^2
\end{aligned}$$

and thus, $D_{JS}^\phi(C_{\mathbb{P}}, C_{\mathbb{Q}}) \geq \frac{1}{8} \|C_{\mathbb{P}} - C_{\mathbb{Q}}\|_*^2 \geq \frac{1}{8} \|C_{\mathbb{P}} - C_{\mathbb{Q}}\|_{\text{HS}}^2$.

Now, let $\phi : \mathcal{X} \mapsto \mathcal{H}$ then, and $\{e_\alpha\}$ be an orthonormal basis in \mathcal{H} , we have that

$$\begin{aligned}
\text{Tr}(\phi(x) \otimes \phi(x)\phi(y) \otimes \phi(y)) &= \sum_{\alpha} \langle \phi(x) \otimes \phi(x)\phi(y) \otimes \phi(y)e_\alpha, e_\alpha \rangle \\
&= \sum_{\alpha} \langle \phi(x) \langle \phi(x), \phi(y) \otimes \phi(y)e_\alpha \rangle, e_\alpha \rangle \\
&= \sum_{\alpha} \langle \phi(x) \langle \phi(x), \phi(y) \langle \phi(y), e_\alpha \rangle \rangle, e_\alpha \rangle \\
&= \sum_{\alpha} \langle \phi(x) \langle \phi(x), \phi(y) \rangle \langle \phi(y), e_\alpha \rangle, e_\alpha \rangle \\
&= \sum_{\alpha} \langle \phi(x), e_\alpha \rangle \langle \phi(x), \phi(y) \rangle \langle \phi(y), e_\alpha \rangle \\
&= \langle \phi(x), \phi(y) \rangle \sum_{\alpha} \langle \phi(x), e_\alpha \rangle \langle \phi(y), e_\alpha \rangle = \langle \phi(x), \phi(y) \rangle \langle \phi(x), \phi(y) \rangle \\
&= \langle \phi(x), \phi(y) \rangle^2 = \kappa(x, y)^2
\end{aligned}$$

Note that for $T : \mathcal{H} \mapsto \mathcal{H}$, $\text{Tr}(T^*T) = \sum_{\alpha} \langle Te_\alpha, Te_\alpha \rangle = \|T\|_{\text{HS}}^2$. In particular, if we have that $T = \phi(x) \otimes \phi(x) - \phi(y) \otimes \phi(y)$,

$$\begin{aligned}
\|\phi(x) \otimes \phi(x) - \phi(y) \otimes \phi(y)\|_{\text{HS}}^2 &= \text{Tr}(\phi(x) \otimes \phi(x)\phi(x) \otimes \phi(x)) - 2 \text{Tr}(\phi(x) \otimes \phi(x)\phi(y) \otimes \phi(y)) \\
&\quad + \text{Tr}(\phi(y) \otimes \phi(y)\phi(y) \otimes \phi(y)) \\
&= \kappa^2(x, x) - 2\kappa^2(x, y) + \kappa^2(y, y)
\end{aligned}$$

Finally, note that

$$\begin{aligned}
\|C_{\mathbb{P}} - C_{\mathbb{Q}}\|_{\text{HS}}^2 &= \text{Tr}(\mathbb{E}_{\mathbb{P}}[\phi(x) \otimes \phi(x)]\mathbb{E}_{\mathbb{P}'}[\phi(x) \otimes \phi(x)]) - 2 \text{Tr}(\mathbb{E}_{\mathbb{P}}[\phi(x) \otimes \phi(x)]\mathbb{E}_{\mathbb{Q}}[\phi(y) \otimes \phi(y)]) \\
&\quad + \text{Tr}(\mathbb{E}_{\mathbb{Q}}[\phi(y) \otimes \phi(y)]\mathbb{E}_{\mathbb{Q}'}[\phi(y) \otimes \phi(y)]) \\
&= \text{Tr}(\mathbb{E}_{\mathbb{P}, \mathbb{P}'}[\phi(x) \otimes \phi(x)\phi(x') \otimes \phi(x')]) - 2 \text{Tr}(\mathbb{E}_{\mathbb{P}, \mathbb{Q}}[\phi(x) \otimes \phi(x)\phi(y) \otimes \phi(y)]) \\
&\quad + \text{Tr}(\mathbb{E}_{\mathbb{Q}, \mathbb{Q}'}[\phi(y) \otimes \phi(y)\phi(y') \otimes \phi(y')]) \\
&= \mathbb{E}_{\mathbb{P}, \mathbb{P}'}[\kappa^2(x, x')] - 2\mathbb{E}_{\mathbb{P}, \mathbb{Q}}[\kappa^2(x, y)] + \mathbb{E}_{\mathbb{Q}, \mathbb{Q}'}[\kappa^2(y, y')],
\end{aligned}$$

which corresponds to MMD with kernel $\kappa^2(\cdot, \cdot)$. \square

A.6 Proof Lemma 1

Proof. Notice that the sum of covariance matrices in the RKHS corresponds to the concatenation of samples in the input space, that is:

$$\begin{aligned}
\pi_1 \mathbf{C}_X + \pi_2 \mathbf{C}_Y &= \frac{1}{N+M} \Phi_X^\top \Phi_X + \frac{1}{N+M} \Phi_Y^\top \Phi_Y \\
&= \frac{1}{N+M} \begin{bmatrix} \Phi_X^\top & \Phi_Y^\top \end{bmatrix} \begin{bmatrix} \Phi_X \\ \Phi_Y \end{bmatrix} \\
&= \frac{1}{N+M} \Phi_Z^\top \Phi_Z = \mathbf{C}_Z,
\end{aligned}$$

where $\Phi_Z = \begin{bmatrix} \Phi_X^\top & \Phi_Y^\top \end{bmatrix}^\top \in \mathbb{R}^{(N+M) \times D}$ contains the mappings of the mixture (concatenation) of the samples in the input space \mathbf{Z} . Since the spectrum of \mathbf{C}_Z and \mathbf{K}_Z have the same non-zero eigenvalues, $S(\pi_1 \mathbf{C}_X + \pi_2 \mathbf{C}_Y) = S(\mathbf{C}_Z) = S(\mathbf{K}_Z)$ \square

B Algorithms

Algorithms 1, 2, and 3 describe the procedure to estimate JS divergence regularly and with Exponential Moving Averages (EMA), and to train GANs based on representation JS divergence.

Algorithm 1 JS divergence estimation

Input: $\mathbf{X} \sim \mathbb{P}, \mathbf{Y} \sim \mathbb{Q}, \eta$

- 1: $\omega \leftarrow$ Initialize network parameters parameters.
- 2: **for** $T = 1$: Number of epochs **do**
- 3: $\Phi_X \leftarrow \phi_\omega \circ f_\omega(\mathbf{X})$
- 4: $\Phi_Y \leftarrow \phi_\omega \circ f_\omega(\mathbf{Y})$
- 5: $\mathbf{C}_X \leftarrow \frac{1}{N} \Phi_X^\top \Phi_X$
- 6: $\mathbf{C}_Y \leftarrow \frac{1}{M} \Phi_Y^\top \Phi_Y$
- 7: $D_{JS}^\omega(\mathbf{X}, \mathbf{Y}) = S(\pi_1 \mathbf{C}_X + \pi_2 \mathbf{C}_Y) - (\pi_1 S(\mathbf{C}_X) + \pi_2 S(\mathbf{C}_Y))$ \triangleright as in Eqn. 13
- 8: $\omega \leftarrow \omega + \eta \nabla_{\text{Adam}} D_{JS}^\omega(\mathbf{X}, \mathbf{Y})$ \triangleright Maximize the divergence
- 9: **end for**

Output: $\widehat{D}_{JS}(\mathbb{P}, \mathbb{Q}) = D_{JS}^\omega(\mathbf{X}, \mathbf{Y})$

Algorithm 2 JS divergence estimation EMA

Input: $\mathbf{X} \sim \mathbb{P}, \mathbf{Y} \sim \mathbb{Q}, \eta, \alpha$

- 1: $\omega \leftarrow$ Initialize network parameters parameters.
- 2: **for** $T = 1$: Number of epochs **do**
- 3: $\Phi_X; \Phi_Y$ \triangleright Compute the mappings
- 4: $\mathbf{C}_X; \mathbf{C}_Y$ \triangleright Compute the covariance matrices
- 5: **if** $T = 1$ **then**
- 6: $\widehat{\mathbf{C}}_X[T] = \mathbf{C}_X$
- 7: $\widehat{\mathbf{C}}_Y[T] = \mathbf{C}_Y$ \triangleright Store previous covariance matrices
- 8: **else**
- 9: $\widehat{\mathbf{C}}_X[T] \leftarrow (1 - \alpha) \widehat{\mathbf{C}}_X[T - 1] + \alpha \mathbf{C}_X$
- 10: $\widehat{\mathbf{C}}_Y[T] \leftarrow (1 - \alpha) \widehat{\mathbf{C}}_Y[T - 1] + \alpha \mathbf{C}_Y$ \triangleright Compute EMA covariance matrices
- 11: **end if**
- 12: $D_{JS}^\omega(\mathbf{X}, \mathbf{Y}) = S(\pi_1 \widehat{\mathbf{C}}_X[T] + \pi_2 \widehat{\mathbf{C}}_Y[T]) - (\pi_1 S(\widehat{\mathbf{C}}_X[T]) + \pi_2 S(\widehat{\mathbf{C}}_Y[T]))$
- 13: $e\omega \leftarrow e\omega + \eta \nabla_{\text{Adam}} D_{JS}^\omega(\mathbf{X}, \mathbf{Y})$ \triangleright Maximize the divergence
- 14: **end for**

Output: $\widehat{D}_{JS}(\mathbb{P}, \mathbb{Q}) = D_{JS}^\omega(\mathbf{X}, \mathbf{Y})$

Algorithm 3 Representation JS divergence GAN

Input: $\mathbf{X}_P = \{\mathbf{X}_i\}_{i=1}^k \sim \mathbb{P}$

- 1: $\theta, \omega \leftarrow$ Initialize network parameters parameters.
 - 2: **for** $T = 1$: Number of epochs **do**
 - 3: **for** $i = 1$: k **do**
 - 4: $\mathbf{Y}_i^\theta = g_\theta(\mathbf{z})$ \triangleright Generated batch from random noise \mathbf{z}
 - 5: $\omega \leftarrow \omega + \eta_d \nabla_{\text{Adam}} D_{JS}^\omega(\mathbf{X}_i, \mathbf{Y}_i^\theta)$ \triangleright Maximize the divergence
 - 6: $\theta \leftarrow \theta - \eta_g \nabla_{\text{Adam}} D_{JS}^\omega(\mathbf{X}_i, \mathbf{Y}_i^\theta)$ \triangleright Minimize the divergence
 - 7: **end for**
 - 8: **end for**
-

C Experiments Implementation Details

C.1 Neural JS divergence estimation

Jensen-Shannon divergence between Cauchy distributions: The Jensen-Shannon for two Cauchy distributions $\mathbb{P} \sim p(x; l_p, s_p)$ and $\mathbb{Q} \sim p(x; l_q, s_q)$ can be estimated as (Nielsen & Okamura, 2022):

Table 2: Architectures mode collapse experiments

Generator	Discriminator	DFFN
Linear(32,256)	Linear(2,256)	Linear(2,256)
Leaky ReLU(0.01)	Leaky ReLU(0.01)	Leaky ReLU(0.01)
Linear(256,256)	Linear(256,256)	Linear(256,256)
Leaky ReLU(0.01)	Leaky ReLU(0.01)	Leaky ReLU(0.01)
Linear(256,256)	Linear(256,256)	Linear(256,256)
Leaky ReLU(0.01)	Leaky ReLU(0.01)	Leaky ReLU(0.01)
Linear(256,256)	Linear(256,256)	Linear(256,256)
tanH()	Leaky ReLU(0.01)	Leaky ReLU(0.01)
Linear(256,2)	Linear(256, 1)	Fourier Features Layer(256, 8)

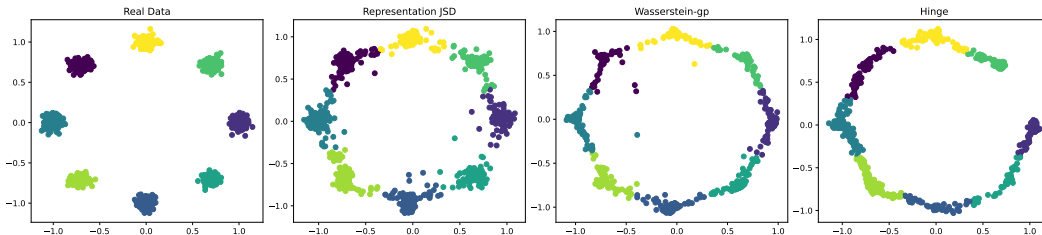


Figure 5: Evaluation of differences between the generated modes and the real modes. The generated data is clustered in 8 modes, and covariances and means are estimated. Then the KL divergence between the real and generated distributions is computed

$$D_{JS}(\mathbb{P}, \mathbb{Q}) = \log \left(\frac{2\sqrt{(l_p - l_q)^2 + (s_p + s_q)^2}}{\sqrt{(l_p - l_q)^2 + (s_p + s_q)^2} + 2\sqrt{s_p s_q}} \right)$$

In this experiment we set $s_p = s_q = 1$, and $l_p = 0$. Then we calculate the value of l_q to achieve a specified divergence value in the set $\{0.2, 0.4, 0.6, 0.8, 0.99\}$.

Implementation details and hyperparameters: Next, we show all the configurations that we used to perform the JS divergence estimation using the representation JS divergence. For this experiment, we use the covariance estimator by using Random Fourier Features (RFFs) to approximate a Gaussian kernel. We chose 50 RFFs and an initial kernel length scale $\sigma = 2$. We set the learning rate as $l_r = 0.001$ and we use the default β_1 and β_2 of the Adam optimizer. We did not use a deep neural network, but the Fourier Features layer by itself. We then applied algorithm 1 to learn ω and σ . We also implemented a version of the algorithm using exponential moving averages (EMA) of the covariance matrices. Specifically, we store information from past covariances and applied EMA to smooth out the estimation. Algorithm 2 shows a detailed explanation of this implementation.

C.2 Generative Adversarial Networks

C.2.1 Mode Collapse experiments

To perform the mode collapse experiments, we used the code provided in https://github.com/ChristophReich1996/Mode_Collapse to compare GAN losses. To make a fair comparison, the generators of the compared losses are the same. The representation JS divergence does not rely on a discriminator or classifier, however, we used a Deep Fourier Features Network (DFFN) with a similar architecture to the discriminator that we used for the compared losses. Table 2 describes in detail the architectures employed.

For the representation JS divergence, we set the learning rate for the discriminator as $l_d = 1 \times 10^{-4}$ and the learning rate of the generator as $l_g = 5 \times 10^{-4}$. For Wasserstein-GP and Hinge losses, we used $l_d = l_g = 1 \times 10^{-4}$. For the standard GAN loss we used $l_d = 5 \times 10^{-4}$ and $l_r = 1 \times 10^{-4}$. We chose random uniform noise $z \sim \mathcal{U}^{32}[0, 1]$.

Table 3: Architecture GAN on stacked MNIST. We use the following notation for the convolutional layers: ConvLayer(input channels, output channels, kernel size, stride, padding)

Generator	DFFN
ConvTranspose2d(100,512,4,1,0)	Conv2d(3, 64, 4, 2, 1)
Batchnorm()	LeakyReLU(0.2)
ReLU()	Conv2d(64, 128, 4, 2, 1)
ConvTranspose2d(512,256,4,2,1)	LeakyReLU(0.2)
Batchnorm()	Conv2d(128, 256, 4, 2, 1)
ReLU()	LeakyReLU(0.2)
ConvTranspose2d(256,128,4,2,1)	Conv2d(256, 512, 4, 2, 1)
Batchnorm()	LeakyReLU(0.2)
ReLU()	Flatten()
ConvTranspose2d(128,64,4,2,1)	Linear(8192, 512)
Batchnorm()	LeakyReLU(0.2)
ReLU()	Linear(512, 256)
ConvTranspose2d(64,3,4,2,1)	Fourier Features Layer (256, 4)
tanH()	

C.2.2 Stacked MNIST implementation details

Next, we describe the architecture and hyperparameters selection that we used to train a GAN in the stacked MNIST dataset, as well as some practical considerations. We used the standard DCGAN generator architecture (Radford et al., 2015) and slightly modified the discriminator architecture to incorporate a Fourier Feature Layer. Table 3 describes in detail the architecture employed. As you can see, we removed all batch norm layers in the discriminator and added two linear layers before the Fourier Feature mapping to reduce the high dimensionality of the last convolutional layer. We resized the images to $64 \times 64 \times 3$ to be compatible with the standard DCGAN architecture.

We draw z from a truncated Gaussian of 100 dimensions, with truncation parameter $\tau = 0.5$, where values that fall outside τ times the standard deviation are resampled to fall inside the range. This is known as the truncation trick.

We set the batch size as 64, and we train the GAN for 15 epochs. We set the discriminator’s learning rate as $l_d = 2.0 \times 10^{-5}$ whereas the generator’s as $l_g = 1.0 \times 10^{-4}$. We chose $\beta_1 = 0.5$ and $\beta_2 = 0.999$ as the hyperparameters of the Adam optimizer.

Here are some practical considerations to train a GAN with the representation JS divergence. First, the learning rates are crucial. If we use a high learning rate for the discriminator, it leads to a 0.99 divergence value, which the generator is not able to reduce. In contrast, if the discriminator’s learning rate is too small, then the divergence will remain close to 0 and the algorithm will not learn. So it is really important to choose the learning rates so that the divergence can grow quickly in the first steps but then the generator should be able to lower the divergence quickly too. Figure 6 shows the loss behavior during training with the selected learning rates. We also observed that a small number of Fourier Features (4 Fourier features, leading to 8 dimensions) lead to better results and make the algorithm easier and faster to train. We observed empirically that a large number of Fourier Features — although they could potentially capture richer information — makes the model prone to overfitting, yielding a high divergence regardless of what the generator does, the divergence stays high.

C.3 Two-sample testing

Procedure details The procedure is the following: for synthetic datasets, we create the sets $\mathbf{X}_{train} \in \mathbb{R}^{N \times d}$ and $\mathbf{Y}_{train} \in \mathbb{R}^{M \times d}$. Then, we learn the kernel/covariance/classifier for each of the methods on that training set. We then sample a testing set $\mathbf{X}_{test} \in \mathbb{R}^{N \times d}$ and $\mathbf{Y}_{test} \in \mathbb{R}^{M \times d}$ and perform a permutation test. We compute the statistic on the testing set and perform 100 permutations to generate the surrogate of the distribution of the measurement under the null hypothesis. Finally, we compute the rejection threshold, and if the statistic is greater than this threshold we reject the null hypothesis. This is done for 100 independent testing sets. Finally, we repeat the experiment ten times and compute the average test power.

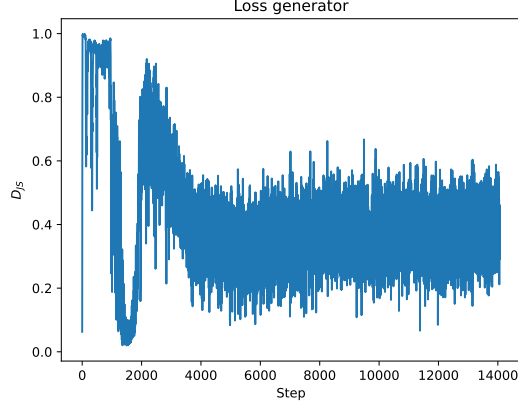


Figure 6: Loss GAN on the stacked MNIST dataset.

RJSD-D test implementation details In this experiment, we try a slightly different implementation of the proposed covariance estimator using a deep Fourier Features network. We explore the idea of deep kernel learning by following a similar approach to Liu et al. (2020), where a characteristic kernel $\kappa_\omega(x, y)$ is built as follows:

$$\kappa_\omega(x, y) = [(1 - \epsilon)\kappa_1(f_\omega(x), f_\omega(y)) + \epsilon]\kappa_2(x, y), \quad (20)$$

$$= (1 - \epsilon)\kappa_1(f_\omega(x), f_\omega(y))\kappa_2(x, y) + \epsilon\kappa_2(x, y) \quad (21)$$

where $f_\omega : \mathcal{X} \rightarrow \mathcal{F}$ is a deep network that extracts features from the data, allowing the kernel to have more flexibility to capture more accurately the structure of complicated distributions. $0 < \epsilon < 1$ and κ_1 and κ_2 are Gaussian kernels. Notice, that the kernel of the deep network features, κ_1 , is multiplied by another kernel κ_2 on the input space. This approach prevents the deep kernel from considering distant points in the input space as very similar.

In this work, we extend this idea to covariance operators and we propose a similar approach to learn deep covariance operators by learning an explicit mapping to the RKHS of a deep kernel. In first place, consider the product $\kappa_p(x, y) = \kappa_1(f_\omega(x), f_\omega(y))\kappa_2(x, y)$. Assuming $\kappa_\sigma = \kappa_1 = \kappa_2$ are Gaussian kernels with bandwidth σ , then $\kappa_p(x, y) = \kappa_\sigma(f_\omega(x) \oplus x, f_\omega(y) \oplus y)$, where \oplus stands for concatenation of the dimensions, that is, κ_p would be the kernel applied to the concatenation of the features from the deep network and the features in the input space. Afterward, we can use Fourier Features to learn an explicit mapping $\phi_\omega : \mathcal{X} \oplus \mathcal{F} \rightarrow \mathcal{H}_\phi$ to approximate a given shift-invariant kernel. Notice, that this approach is nothing but a linear layer with random weights $e_\omega \sim p(e_\omega)$ and sines and cosines as activation functions. Therefore $\kappa_p(x, y) \approx \langle \phi_\omega(f_\omega(x) \oplus x), \phi_\omega(f_\omega(y) \oplus y) \rangle_{\mathcal{H}_\phi}$. $\kappa_2(x, y)$ can be similarly approximated through a Fourier Feature mapping $\psi_\omega : \mathcal{X} \rightarrow \mathcal{H}_\psi$ applied directly on the samples in the input space, that is $\kappa_2(x, y) \approx \langle \psi_\omega(x), \psi_\omega(y) \rangle_{\mathcal{H}_\psi}$.

Finally, consider the whole kernel $\kappa_\omega(x, y) = (1 - \epsilon)\kappa_p(x, y) + \epsilon\kappa_2(x, y)$, which is the direct sum of two kernels with approximated explicit mappings ϕ_ω and ψ_ω respectively. By the properties of RKHS, it can be shown that:

$$\begin{aligned} \kappa_\omega(x, y) &= (1 - \epsilon)\kappa_p(x, y) + \epsilon\kappa_2(x, y) \\ &\approx \langle \varphi_\omega(x), \varphi_\omega(y) \rangle_{\mathcal{H}}, \end{aligned} \quad (22)$$

where $\varphi_\omega(x) = \left[(1 - \epsilon)^{\frac{1}{2}} \phi_\omega(x') \right] \oplus \left[\epsilon^{\frac{1}{2}} \psi_\omega(x) \right]$, $\mathcal{H} = \mathcal{H}_\psi \oplus \mathcal{H}_\phi$ and $x' = f_\omega(x) \oplus x$.

This procedure allows us to obtain an explicit mapping to the RKHS from a deep kernel that can be used to compute an explicit covariance operator. Consequently, this covariance operator can be optimized to maximize the JS divergence between the distributions. Note, that we can learn the parameters of the network f_ω as well as the Fourier Features e_ω and the kernel bandwidth σ .

Table 4: Architecture of the Deep Fourier Features Network (DFFN) and the Deep Convolutional Fourier Features Network(DCFFN) used in two sample testing. d is the input dimensionality, H is the number of hidden neurons and FF is the number of Fourier Features. The Convolutional Layers follow the same notation as 3

DFFN	DCFFN (MNIST)
Linear(d, H)	Conv2d(3,16,3,2,1)
Softplus()	LeakyReLU(0.2)
Linear(H, H)	Conv2d(16,32,3,2,1)
Softplus()	LeakyReLU(0.2)
Linear(H, H)	Conv2d(32,64,3,2,1)
Softplus()	LeakyReLU(0.2)
Linear(H, H)	Conv2d(64,128,3,2,1)
Fourier Features Layer (H, FF)	LeakyReLU(0.2)
	Linear (128,512)
	ReLU
	Linear (512,100)

Two-sample testing implementation details We run all baselines using the official implementation, that is MMD-O and MMD-D (Liu et al., 2020)², C2ST-S and C2ST-L (Cheng & Cloninger, 2022)³. We follow all the configuration and architecture proposed by Liu et al. (2020). To perform RJSD-D, we used the same architecture as MMD-D, although, we add a Fourier Feature layer where MMD-D computes a kernel. Table 4 shows the details of the architecture used. The base network consists of five fully connected layers, and the number of neurons in hidden and output layers is set to 50 for Blob, $3 \times d$ for HDGM, and 20 for the Higgs dataset, where d is the dimension of the dataset. Also, the number of Fourier Features for all JSD-based tests is set to 50 for Blob, 15 for HDGM, and 15 for the Higgs dataset.

Two-sample testing implementation details on MNIST DCFFN is the model used on MNIST and it is described in Table 4. This model is the same proposed by Liu et al. (2020) except that we remove the batch normalization layers between the convolutional layers. For RJSD-D, we set the batch size to 100 and the number of epochs to 200 for MNIST. We set the learning rate to 0.05 for MNIST. We set the number of Fourier Features to 10 for MNIST.

For RJSD-RFF, we use full batch size to train it. We set the number of epochs to 200 for MNIST. We set the learning rate to 0.01 for MNIST and 0.001. We set the number of Fourier Features to 200 for MNIST.

For RJSD-FF, we use full batch size to train it. We set the number of epochs to 200 for MNIST. We set the learning rate to 0.05 for MNIST.

We use Adam optimizer to optimize 1) The kernel length scale σ in RJSD-K and RJSD-RFF 2) the Fourier Features ω and kernel length scale σ in RJSD-FF and 3) the network parameters $\omega \in \Omega$, the Fourier Features ω and the kernel length scale σ in RJSD-D. For the blobs dataset, we set the learning rate of RJSD-FF, RJSD-RFF and RJSD-D as $l_r = 1 \times 10^{-3}$. For the HDGM, we set the learning rate for RJSD-FF and RJSD-RFF as $l_r = 5 \times 10^{-3}$, and the one for RJSD-D as $l_r = 5 \times 10^{-2}$. In the Higgs dataset, we set all the learning rates as $l_r = 1 \times 10^{-2}$.

Figures 7,8,9,10 show the average test power and the standard deviation of each of the implemented test.

C.4 Limitations

Although the representation Jensen-Shannon divergence shows promising results, there are still some aspects that require further research. So far, the number of Fourier Features to build the reproducing kernel Hilbert space (RKHS) has been chosen arbitrarily. Empirically, we have found that choosing $D \ll N$ usually leads to better results, which could seem counter-intuitive with the kernel theory that usually induces a high-dimensional space. Also, using the kernel-based estimator

²<https://github.com/fengliu90/DK-for-TST>

³https://github.com/xycheng/net_logit_test/tree/main

for maximization purposes would require enforcing constraints on the scale of the data since this estimator can potentially exhibit rank-inconsistency of the matrices, that is $\max \text{Rank}(\mathbf{K}_Z) = N + M$, $\max \text{Rank}(\mathbf{K}_X) = N$ and $\max \text{Rank}(\mathbf{K}_Y) = M$. If the data scale is not kept fixed, trivial maximization of the divergence by just spreading all the samples far apart in the space, or equivalently for a Gaussian kernel by decreasing the length-scale σ can occur. For this reason, we employed the covariance-based estimator with a finite dimension (explicit feature space) in most of our experiments.

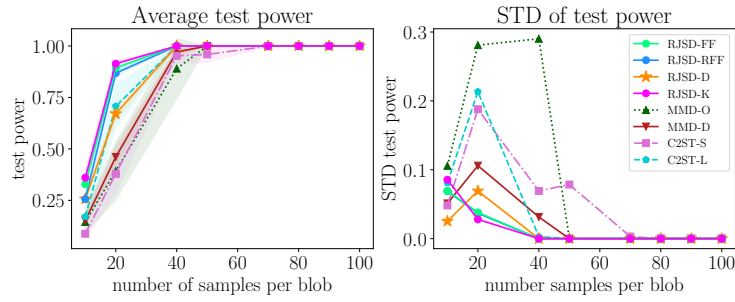


Figure 7: Power test for the blobs experiment.

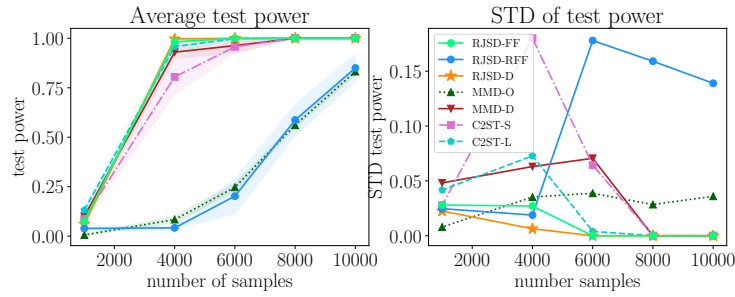


Figure 8: Power test for HDGM fixed N.

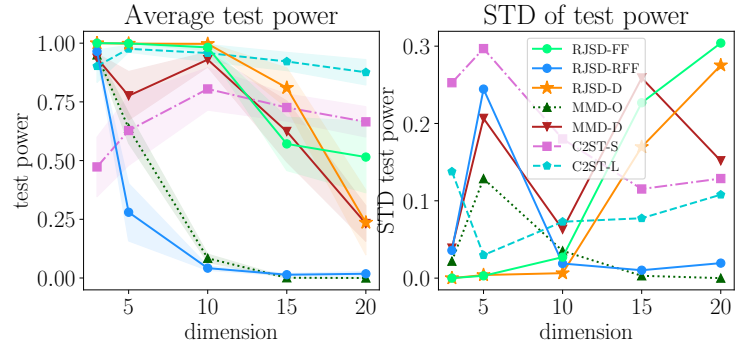


Figure 9: Power test for HDGM fixed d.

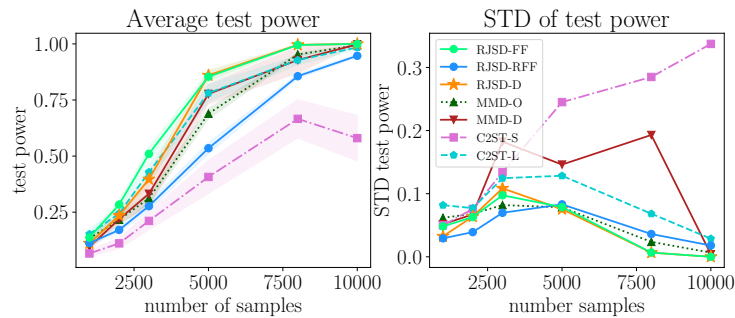


Figure 10: Power test for the Higgs dataset.